UFM1 E3 ligase promotes recycling of 60S ribosomal subunits from the ER

DaRosa, Paul A.; Penchev, Ivan; Gumbin, Samantha C.; Scavone, Francesco; Wąchalska, Magda; Paulo, Joao A.

Published in:
Nature

DOI:
10.1038/s41586-024-07073-0

Publication date:
2024

Document Version
Peer reviewed version

UFM1 E3 ligase promotes recycling of 60S ribosomal subunits from the ER

Paul A. DaRosa[1#], Ivan Penchev[2#], Samantha C. Gumbin[1], Francesco Scavone[1], Magda Wąchalska[1], Joao A. Paulo[3], Alban Ordureau[3,4], Joshua J. Peter[5], Yogesh Kulathu[5], J. Wade Harper[3], Thomas Becker[2], Roland Beckmann[2,*] and Ron R. Kopito[1,*]

# equal contributions

[1]Department of Biology, Stanford University, Stanford, CA, United States

[2]Department of Biochemistry, Gene Center, Feodor-Lynen-Str. 25, University of Munich, 81377 Munich, Germany.

[3]Department of Cell Biology, Harvard Medical School, Boston, MA, United States

[4]Present address: Cell Biology Program, Sloan Kettering Institute, Memorial Sloan Kettering Cancer Center, New York, NY 10065, USA

[5]Medical Research Council Protein Phosphorylation & Ubiquitylation Unit (MRC-PPU), School of Life Sciences, University of Dundee, Dundee, UK.

*Corresponding authors:

Ron R Kopito. Email: kopito@stanford.edu

Roland Beckmann. Email: beckmann@genzentrum.lmu.de

This version of the article has been accepted for publication, after peer review and is subject to Springer Nature's AM terms of use, but is not the Version of Record and does not reflect post-acceptance improvements, or any corrections. The Version of Record is available online at: http://dx.doi.org/10.1038/s41586-024-07073-0.

Abstract:

Reversible modification of target proteins by ubiquitin and ubiquitin-like proteins (Ubl) is widely used by eukaryotic cells to control protein fate and cell behavior[1]. UFM1 is a Ubl that predominantly modifies a single lysine residue on a single ribosomal protein, uL24 (also called RPL26), on ribosomes at the cytoplasmic surface of the endoplasmic reticulum (ER)[2,3]. UFM1 conjugation (UFMylation) facilitates rescue of 60S subunits that are released upon ribosome-associated quality control (RQC)-mediated splitting of ribosomes that stall during co-translational translocation of secretory proteins into the ER[3,4]. Neither the molecular mechanism by which the UFMylation machinery achieves such precise target selection, nor how this ribosomal modification promotes 60S rescue is known. Here, we show that ribosome UFMylation *in vivo* occurs on free 60S ribosomal subunits and present sequential cryo-electron microscopic snapshots of the heterotrimeric E3 UFM1 ligase ($E3^{UFM1}$) engaging its substrate, uL24. $E3^{UFM1}$ binds to the L1 stalk, empty tRNA binding sites, and the peptidyl transferase center (PTC) via C-terminal domains of UFL1, resulting in uL24 modification more than 150 Å away. After catalyzing UFM1 transfer, $E3^{UFM1}$ remains stably bound to its product, UFMylated 60S, forming a C-shaped clamp that extends all the way around the 60S from the tRNA binding sites to the polypeptide tunnel exit. Our structural and biochemical analyses suggest a role for $E3^{UFM1}$ in post-termination release and recycling of the large ribosomal subunit from the ER membrane.

MAIN:

UFM1, like other Ubls, is conjugated to its targets by a canonical E1-E2-E3 enzymatic cascade, where the E3 ligase specifies target selection[5]. $E3^{UFM1}$ is a scaffold-type ligase, composed of a stoichiometric assembly of three subunits: UFL1, DDRGK1 (also known as UFBP1 or C20orf116), and CDK5RAP3 none of which share common motifs or homologies with other Ub or Ubl E3 ligases[6]. Two subunits, UFL1 and DDRGK1, are composed predominantly of predicted winged helix (WH) motifs, and comprise the minimal E3 ligase catalytic unit[6,7]. CDK5RAP3 is not essential for E3 ligase activity *in vitro* but appears to function as a substrate adaptor or selectivity factor that constrains $E3^{UFM1}$ ligase activity to mono-UFMylate the ribosomal protein uL24/RPL26 on lysine residue K134 (ref. [6]). A transmembrane domain on DDRGK1 tethers $E3^{UFM1}$ to the ER membrane, restricting $E3^{UFM1}$ activity to ER-docked ribosomes[2]. Accordingly, UFMylation is strongly linked to maintenance of protein homeostasis in the ER[8,9].

Although the function of uL24 on the ribosome is not well-understood, its localization at the polypeptide tunnel exit on the 60S ribosomal subunit (60S) places the site of UFM1 modification at a strategic position to influence the interaction between ER-bound ribosomes and the SEC61 translocon[2]. UFMylation of uL24 is increased upon ER-specific ribosome stalling[3,4] and is essential for RQC-dependent degradation of partially translocated, nascent "arrest peptides" (ER-APs) that obstruct both the ribosome exit tunnel and the SEC61 translocon following splitting of ribosomes[4]. These data led us to propose that uL24 UFMylation weakens the junction between post-termination 60S subunits and SEC61 translocons, allowing cytosolic ubiquitin-proteasome system (UPS) machinery to access ER-APs that are otherwise occluded by the tight ribosome-translocon junction[4]. A key feature of this model is the existence of an unidentified UFMylation

65 "reader" that recognizes the uL24-conjugated UFM1 moiety and induces a conformational change
66 that disrupts the tight interaction between SEC61 and terminated 60S.
67
68 **Association of E3^{UFM1} with UFMylated 60S**
69 To identify potential UFMylation readers in the ER membrane, we used proximity labeling,
70 with "miniTurbo" (mT)[10] fused to the N-terminus of UFM1 (mT-UFM1) knocked into the
71 endogenous *UFM1* locus (**Extended Data Fig. 1a**). Control experiments confirmed that the
72 predominant cellular target of mT-UFM1 is uL24 and that adduct formation was abrogated in E1
73 knockout (*UBA5*^{KO}) cells (**Extended Data Fig. 1b-d**) and greatly enhanced in cells lacking the
74 ER membrane-tethered deUFMylase, UFSP2 (ref. [2,11]) (**Extended Data Fig. 1b**). Furthermore,
75 uL24 modification with mT-UFM1 was stimulated by inducing ribosome collisions with sub-
76 stoichiometric concentrations of anisomycin (ANS) and mT-UFM1-modified uL24 co-sedimented
77 with ribosomes (**Extended Data Fig. 1c**). Thus, mT-UFM1 mimics the biochemical properties of
78 untagged UFM1, making it a suitable probe to analyze the UFM1 proximitome. Because the
79 steady-state level of UFM1 conjugates in cells is low compared to that of free UFM1 (ref. [2]), we
80 used a workflow that allowed for statistically robust, direct comparison of total mT-UFM1-
81 proximal proteins captured from wild-type cells with those identified in UFMylation-deficient
82 *UBA5*^{KO} cells (**Extended Data Fig. 1a**). This approach was validated in control experiments
83 showing that biotin modification of the UFMylation E2 enzyme, UFC1, which forms thioester and
84 peptidyl adducts with UFM1 (ref. [12]), was completely abrogated in *UBA5*^{KO} cells (**Extended Data**
85 **Fig. 1d**) and in the full dataset (**Fig. 1a**). In total, we quantified 2213 streptavidin-enriched proteins
86 (**Supplementary Table 1**) of which 54 (2.4%) were significantly and robustly (over two-fold)
87 affected upon UBA5 deletion (**Fig. 1a and Supplementary Table 1**). Significant hits were

enriched for ER membrane-localized proteins, including components of the translocation, ER-targeting, and N-glycosylation machinery (**Fig. 1a**), consistent with restriction of UFM1 conjugation to 60S ribosomal subunits docked at ER membrane translocons[2]. While the proximity labeling approach failed to identify novel ER-membrane proteins that could be considered as plausible candidates for a UFM1 reader, we noted that $E3^{UFM1}$ subunits ranked among the most highly enriched (>8 fold) and statistically significant ($P < 10^{-9}$) proteins, suggesting that the membrane-tethered $E3^{UFM1}$ itself could potentially function as a reader for UFMylated ribosomes at the ER membrane. Indeed, all three $E3^{UFM1}$ subunits were strongly enriched in MS/MS-analysis of streptavidin binding peptide (SBP)-UFM1 affinity-captured material from *UFSP2*^{KO} cells (**Fig. 1b, c and Extended Data Fig. 1e)**, strongly suggesting that this E3 enzyme complex remains bound to 60S after catalyzing UFM1 transfer to uL24. The strong enrichment for proteins involved in 60S recycling and biogenesis (eIF6, ZNF622, PA2G4, GTPBP4, and NMD3), is consonant with a role for UFMylation in recycling of 60S subunits following collision-induced stalling of ribosomes engaged in co-translational translocation at the ER[3,4], and with data from genome-wide co-essentiality network analysis (**Extended Data Fig. 2a, b**).

To understand this surprisingly persistent interaction of $E3^{UFM1}$ with UFMylated 60S, the product of the conjugation reaction it catalyzes, we analyzed the distribution of UFMylated uL24 and $E3^{UFM1}$ subunits on sucrose density gradients of whole cell lysates (**Extended Data Fig. 1f-h**) or membrane fractions (**Fig. 1d and Extended Data Fig. 1i, j**) from K562 cells. UFMylated uL24 and $E3^{UFM1}$ co-sedimented with 60S fractions from wildtype cells, (**Fig. 1d, *left panel* and Extended Data Fig. 1f-h**) consistent with prolonged association between $E3^{UFM1}$ and UFMylated ribosomes. The finding that eIF6 and NEMF - proteins that bind to the subunit interface on free 60S[13–17] - co-sedimented with UFMylated uL24 and $E3^{UFM1}$ (**Fig. 1d and Extended Data Fig. 1g,**

quantified in Extended Data Fig. 1h) suggests that in cells, $E3^{UFM1}$ and UFMylated uL24 associate predominantly with free 60S. The loss of $E3^{UFM1}$ association with ribosomes in *UFM1*^{KO} cells (**Fig. 1d, *middle panel***) suggests that this ligase binds more persistently to UFMylated than to unmodified 60S. Conversely, inducing ribosome collisions with anisomycin (**Extended Data Fig. 1k, l**) or inactivating UFSP2, manipulations which increase the fraction of UFMylated 60S (**Fig. 1d, *right panel***), resulted in proportionately increased association of $E3^{UFM1}$ subunits with 60S. These data, together with the finding that all three $E3^{UFM1}$ subunits co-sediment with 60S following *in vitro* UFMylation reconstitution with purified, soluble, recombinant E1, E2, and E3[6] (**Fig. 1e**) in the presence, but not the absence of ATP, confirm that uL24 UFMylation is both necessary and sufficient for persistent association of $E3^{UFM1}$ with 60S. When purified salt-washed 60S or 80S were added to an *in vitro* UFMylation assay, 60S were far more rapidly modified than 80S (**Fig. 1f**), even in the presence of a 2-fold excess of 80S (**Extended Data Fig. 1m**). By contrast, 80S ribosomes are far less efficiently UFMylated in the cell-free assay (**Extended Data Fig. 1n**). Together, these data reveal that uL24 on free 60S subunits is the preferred substrate of UFMylation.

Architecture of the 60S-$E3^{UFM1}$ complex

As expected from the preceding analysis, FLAG-UFM1 affinity-captured material was heavily enriched for 60S ribosomal proteins and all three $E3^{UFM1}$ subunits (**Fig. 2a**). Single particle cryo-electron microscopy (Cryo-EM) analysis of this material (**Extended Data Fig. 3a**) identified 60S with extraribosomal densities that could be assigned to eIF6 (**Fig. 2b**). Several additional classes contained continuous density that was assigned to UFM1 (near uL24) and the $E3^{UFM1}$ complex with the best-resolved 60S class refined to 3.1 Å (**Fig. 2b, Extended Data Fig. 4a, and**

Extended Data Table 1). Cryo-EM analysis of *in vitro* UFMylated 60S (**Extended Data Fig. 3b**) yielded an essentially identical 3D reconstruction (lacking eIF6) of the 60S-UFM1-E3^{UFM1} complex at a somewhat higher resolution of 2.9 Å (**Fig. 2c-e, and Extended Data Fig. 4a**). The region around uL24 and the tunnel exit exhibited even higher local resolution, ranging from 2.3 Å for the ribosomal core to 3-7 Å for the UFM1-E3^{UFM1} complex (**Extended Data Fig. 4b, c**). In both native and *in vitro* reconstituted complexes, E3^{UFM1} adopted the same elongated clamp-like configuration, spanning from the tunnel exit (**Fig. 2d, e**) to the empty tRNA binding sites (**Fig. 2f**). These data, in combination with AlphaFold 2 (ref. [18]) and AlphaFold-Multimer[19] structure predictions allowed us to build a near-complete molecular model of 60S-UFM1-E3^{UFM1} (**Fig. 2g, Extended Data Fig. 5a-c, Extended Data Fig. 6, and Extended Data Table 1**).

Molecular model of the 60S-E3^{UFM1} complex

The 60S-UFM1-E3^{UFM1} molecular model reveals the overall structure and interactions of E3^{UFM1} and suggests how it can read the UFM1 modification on 60S (**Fig. 3a, b**). While the local resolution of UFM1 is relatively low, it is positioned over its substrate uL24 near its known conjugation site at K134[2,3] (**Fig. 3b, and Extended Data Fig. 6c**). Notably, UFM1 is not in direct contact with UFL1 but instead with DDRGK1 and CDK5RAP3, which, in turn, form an intricate interaction network and a well-ordered complex with UFL1 (**Fig. 3a, b, and Extended Data Fig. 6b**).

In this E3^{UFM1} complex, UFL1 serves as a central scaffold that consists of a predicted short N-terminal α-helix followed by one partial winged-helix (pWH), five WH motifs, a bipartite coiled-coil domain (CC) with a disordered region that reaches into the PTC and bridges the two helices, and a C-terminal globular domain (**Fig. 3a-c, and Extended Data Fig. 6a, b**). DDRGK1

157 contains an N-terminal transmembrane (TM) domain and a flexible linker region (between
158 residues 1-118) that were not visualized in our reconstructions. The remainder of DDRGK1
159 consists of a long α-helix [amino acids (AAs) 119-195], connected via a short linker (AAs 196-
160 208) to a WH motif, and a pWH. The latter complements the N-terminal pWH domain of UFL1
161 to form a composite WH, thereby linking these two subunits to form the backbone of the minimal
162 E3 ligase complex[6]. The CDK5RAP3 subunit of $E3^{UFM1}$ packs against the UFL1/DDRGK1
163 backbone via a long coiled-coil (CC) domain flanked by two globular domains, GD1 and GD2.
164 GD1 contacts the N-terminal α-helix of UFL1, whereas GD2 interacts with WH2 and WH3 of
165 UFL1, together giving rise to an overall C-shaped appearance of $E3^{UFM1}$ (**Fig. 3b**).
166 The interaction of $E3^{UFM1}$ with 60S is multimodal, with contributions from all three
167 subunits. The C-terminal globular domain of UFL1 is sandwiched between 28S rRNA helices H38
168 and H69 most likely through complementary charges (**Fig. 3c**). These helices constitute
169 functionally important sites in the active 80S ribosome, namely the A-site finger (H38), which
170 coordinates the A site tRNAs, and the main intersubunit bridge B2A (between H69 and 18S rRNA
171 helix h44). As a result, the C-terminal domains of UFL1 occlude all three tRNA binding sites (**Fig.**
172 **2d**). In addition, a small helix and loop (PTC-loop) of the UFL1 disordered region are positioned
173 in the P-site near the PTC where the conformation of the PTC base U4452 (U2506 of *E. coli*) is
174 remodeled (**Fig. 3b, f**) and UFL1 Y443's aromatic ring is stacked upon A4548 (A2602 in *E. coli*).
175 This binding mode of $E3^{UFM1}$ is therefore mutually exclusive with any tRNA binding. The most
176 intimate interaction of UFL1 with 60S occurs near the E-site and with the ribosomal L1 stalk,
177 where WH4 and WH5 of UFL1 and GD2 of CDK5RAP3 share extensive contacts which stabilize
178 this otherwise flexible element (**Fig. 3b**). The WH-backbone, composed of the C-terminal WH
179 domains of DDRGK1 and UFL1, and the CC region of CDK5RAP3, reaches towards uL24 (**Fig.**

3b), displacing the tip of rRNA segment H25/ES7a and the C-terminal α−helix of uL13, both of which form contacts with UFL1. From uL24, the long α-helix of DDRGK1 (exit-binding helix; EBH) stretches all the way to the tunnel exit. Its positively charged N-terminal end (designated as exit binding motif; EBM; **Fig. 3a, d**) is positioned on rRNA H47 and H24 (**Fig. 3b, d**), which are part of the binding site for exit site factors such as SRP, SRP receptor (SR), and SEC61 (ref. [20,21]). Across from uL24, the short linker of DDRGK1 (AAs 196-208) between the EBH (AAs 119-195) and the WH domain (AAs 209-272) contains a conserved UFM1-interacting motif (UFIM; **Extended Data Fig. 5d**)[22] that is predicted by AlphaFold-Multimer to interact with UFM1 via β-augmentation (**Fig. 3a, b, e, Extended Data Fig. 5e, f, and Extended Data Fig. 6c**). Although the cryo-EM density map displayed an overall lower local resolution in this region (~7-8 Å; **Extended Data Fig. 4b**), and we cannot exclude a different mode of interaction, the AlphaFold model is supported by good agreement with corresponding density in our map (**Extended Data Fig. 6c**), by its similarity to the β-augmented interaction of UBA5 with UFM1 (ref. [23]) (**Extended Data Fig. 5g**) and by site-directed mutagenesis (see below). Together, these data suggest a model in which uL24-conjugated UFM1 forms the nexus of an intimate interaction network that allows $E3^{UFM1}$ to "read" the 60S modification.

The mono-UFMylated 60S particles observed in our native cryo-EM structures from the UFM1 pulldown clearly represent a state of the 60S devoid of peptidyl-tRNA or nascent chains as occurring during (cytoplasmic) RQC. Furthermore, the positioning of DDRGK1's EBM at the universal binding site of the tunnel exit is likely to preclude binding of SEC61. This, together with the presence of eIF6 in the native structure, indicates that the observed particle represents a post-termination 60S subunit after dissociation from SEC61.

UFL1 C-terminus initiates 60S engagement

FLAG-UFL1 pulldowns were also strongly enriched for all three subunits of $E3^{UFM1}$ (**Fig. 4a**). Single particle cryo-EM analysis of this material exhibited substantially higher heterogeneity compared to FLAG-UFM1 pulldowns, the most striking feature of which was the presence of the SEC61 complex at the tunnel exit in a subset of particles (**Fig. 4b and Extended Data Fig. 4, 7, 8**). 3D classification of the FLAG-UFL1-captured particles revealed three distinct states of $E3^{UFM1}$-60S interaction, with the most populated state, State 3 (**Fig. 4b**), being largely indistinguishable from the post-UFMylation state observed in FLAG-UFM1-pulldowns and *in vitro* UFMylated 60S, but at a higher local resolution for many regions of the E3 (**Fig. 4b and Extended Data Fig. 4, 7**). One feature of the UFL1-captured 60S was a weak extra density in the peptide exit tunnel, which might represent a nascent polypeptide chain or an exit tunnel-binding factor. Notably, states 1 and 2 were bound to SEC61 and exhibited more restricted interaction surfaces with $E3^{UFM1}$. We propose that States 1 and 2 represent SEC61-bound states that exist before and after UFM1 conjugation, respectively. In the State 1 complex, we observed density only for the UFL1 C-terminal region (CTD, CC, WH4, and WH5) occupying the tRNA-binding sites, and the UFL1-CDK5RAP3 region protruding from the ribosome near the L1 stalk (**Fig. 4b**). No density was observed for UFM1 or the rest of $E3^{UFM1}$ in the uL24 region, and rRNA H25ES7 was in its canonical position. By contrast, in State 2, we observed uL24 already UFMylated and $E3^{UFM1}$ almost fully accommodated as in State 3, yet the N-terminal EBH of DDRGK1 was not visible and SEC61 was still present at the tunnel exit (**Fig. 4b**).

As the C-terminal region of UFL1, including the PTC loop, is present in all three states, we suggest that the first step of 60S recognition by $E3^{UFM1}$ is the binding of the UFL1 C-terminal regions to the L1 stalk and/or to a tRNA-free intersubunit surface. UFMylation of uL24 then

eventually leads to rigid positioning of the DDRGK1 N-terminus, including the EBH at the tunnel exit. This positioning appears to be mutually exclusive with SEC61 binding since we never observed the EBH together with SEC61 in the same particle.

To test the role of UFL1's C-terminus in initiating engagement of $E3^{UFM1}$ with 60S, we evaluated the impact on uL24 UFMylation of replacing endogenous UFL1 with UFL1 variants harboring progressive C-terminal UFL1 truncations (**Fig. 4c and Extended Data Fig. 5i**). While deletion of the globular CTD alone (UFL1(1-532); ΔCTD) still supported detectable, albeit reduced UFMylation, further deletion of the CTD-proximal CC helix, together with part of the adjoining disordered domain (UFL1(1-410)), caused near complete abrogation of UFMylation as did a more extensive truncation (UFL1(1-116)). These results confirm the importance of the precise packing of the CTD between 28S rRNA helices H38 and H69 (**Fig. 3c**) and, further, suggest a role for the CC and potentially, the disordered regions including the PTC loop, in stabilizing the initial encounter between $E3^{UFM1}$ and 60S. These results differ from those of Peter et al.[6], who reported that 60S UFMylation, reconstituted *in vitro,* was unaffected by the Δ411-794 deletion, likely reflecting either kinetic or stoichiometric differences between these two experimental paradigms, or perhaps the influence of factors unique to the cellular environment that are absent in the cell-free reconstitutions. The importance of the UFL1 C-terminus in targeting the E3 to ribosomes in the cell may provide an explanation for the preference for 60S as this region is not accessible in 80S ribosomes.

uL24 UFMylation displaces SEC61 from 60S

To test the role of EBM and UFIM in UFMylation, we expressed wildtype DDRGK1 or variants that disrupt either the EBM (Δ119-145; ΔEBM) (**Fig. 3a, d, and Extended Data Fig. 5h**)

or the UFIM (UFIM^{mt}; F196V, V198A, E201P) in *DDRGK1*^{KO} cells (**Fig. 3a, e, and Extended Data Fig. 5f**). Deleting the EBM slightly increased uL24 UFMylation (**Fig. 4d, *left panel***), but had no discernible effect on co-sedimentation of E3^{UFM1} with 60S (**Extended Data Fig. 9c, d**). By contrast, UFIM disruption completely abrogated the stable E3^{UFM1}-ribosome association while enhancing uL24 UFMylation (**Fig. 4d, *left panel* and Extended Data Fig. 9 c, d**). The increased uL24 UFMylation observed in cells expressing UFIM^{mt} likely reflects enhanced dissociation of the mutant E3 from its UFMylated 60S product, allowing the mutant enzyme to modify more ribosomes. This interpretation is reinforced by the observation that a substantial fraction (~50%) of UFMylated uL24 in UFIM^{mt} -expressing cells was associated with cytosolic ribosomes compared to wildtype HEK293 cells or *DDRGK1*^{KO} cells rescued with wildtype DDRGK1 or DDRGK1$^{\Delta EBM}$, in which the vast majority of UFMylated uL24 is on ER-bound ribosomes (**Fig. 4d, *right panel***). These data strongly support the conclusion that β-augmentation between UFM1 and DDRGK1 is strictly required for persistent binding of E3^{UFM1} to its UFMylated product on 60S and further suggest that this interaction facilitates positioning of EBM near the tunnel exit to promote dissociation of SEC61 from ribosomes. In addition to the direct displacement of SEC61 by the DDRGK1 EBM (**Extended Data Fig. 9a, b**), the orientation of E3^{UFM1}, as observed in State 3, would clash with the ER membrane phospholipid bilayer, as visualized in cryo-electron tomography maps of mammalian ER-membrane-bound 80S ribosomes[24] (**Extended Data Fig. 9e, f**). Accommodation of the State 3 E3^{UFM1} thus requires re-orientation of 60S with respect to the ER membrane by a backward tilt that is likely to further destabilize the ribosome-SEC61 interaction.

To directly test the role of UFMylation in promoting SEC61-60S dissociation, we used co-sedimentation of detergent-solubilized SEC61 with ribosomal subunits following forced

termination with puromycin (Puro) (**Fig. 4e and Extended Data Fig. 9g**) or run-off translation in the presence of harringtonine (HT) **(Fig. 4f and Extended Data Fig. 9h, i**) to monitor the effect of disrupting UFMylation on the translocon-ribosome dissociation kinetics. In WT cells we found that SEC61 dissociated from ribosomes with a half-time of ~1 and 15 min, following treatment with Puro or HT, respectively. By contrast, in UFMylation-defective *UFC1*^{KO} (**Fig. 4e, f, and Extended Data Fig. 9g, h**) and *UFM1*^{KO} cells (**Extended Data Fig. 9i**), no significant dissociation of SEC61 was detected over 30 min. These data strongly support the conclusion that UFM1 conjugation is required for timely dissociation of 60S subunits from translocons following termination.

To assess the importance of ribosome dissociation in ER-RQC, we asked if DDRGK1's EBM and UFIM are functionally required for the degradation of an arrest peptide (AP) from an ER-targeted reporter (SS^{VgV}K20)[4] containing a polylysine (K20) tract to mimic "nonstop" translation into a poly(A). Ribosomes translating this reporter initiate co-translational ER translocation of the nascent chain through SEC61, but stall when they encounter the downstream K20 tract[4]. Collision-induced splitting of the stalled ribosome yields an ER-docked 60S-tRNA-AP (ER-AP) complex while the presence of an N-glycan confirms that the arrested nascent chain spans from the P-site through SEC61 into the ER lumen (**Fig. 4g**). We recently reported that uL24 UFMylation of on these 60S-tRNA-AP complexes is essential for the ubiquitin-proteasome system (UPS) to degrade these SEC61- and 60S-obstructing ER-APs, leading us to propose that recognition of the UFM1 mark by a UFM1 reader weakens the junction between 60S and the translocon, allowing cytosolic UPS machinery to access the ER-AP[4]. Here, we find that ER-AP stabilization observed upon *DDRGK1* knockout was fully reversed by re-expression of wildtype DDRGK1 but not by expression of either UFIM^{mt} or ΔEBM variants (**Fig. 4h, i**). Thus, formation

of a stable 60S-UFM1-E3^{UFM1} complex and precise positioning of the DDRGK1 EBM at the tunnel exit are essential for ER-AP degradation, supporting the hypothesis that E3^{UFM1} reads the UFM1 mark on 60S to destabilize the ribosome-SEC61 junction on ER-stalled 60S-tRNA-AP complexes, allowing UPS machinery to extract and degrade these partially translocated ER-APs.

De-UFMylation dissociates 60S and E3^{UFM1}

We propose that hydrolysis of the isopeptide bond linking UFM1 to uL24 by UFSP2, an ER-tethered UFM1-specific hydrolase[2,11], enables simultaneous release of 60S and recycling of UFM1 and E3^{UFM1}. Accordingly, genetic ablation of *UFSP2* leads to a substantial increase in UFMylation of membrane-associated uL24 (ref.[2,3]), and to a corresponding increase in co-sedimentation of E3^{UFM1} with 60S (**Fig. 1d**). The most direct test of the hypothesis that de-UFMylation is necessary and sufficient to promote release of UFMylated 60S from E3^{UFM1}, is to assess the effect of adding purified deUFMylase to the stability of E3^{UFM1}-60S complexes *in vitro*. Because UFSP2 is unstable when separated from its oligomeric partner and membrane anchor, ODR4 (ref. [2]), we treated lysates of *UFSP2*^{KO} cells (**Fig. 5a**) or *in vitro* UFMylated, E3^{UFM1}-bound 60S (**Fig. 5b**) with purified recombinant UFSP1, a cytosolic UFSP2 orthologue with similar substrate selectivity[11], and assessed E3^{UFM1}-60S complex stability by sucrose gradient fractionation. Treatment with UFSP1, but not with NEM-inactivated UFSP1, substantially reduced both uL24 UFMylation and co-sedimentation of E3^{UFM1} subunits with 60S (**Fig. 5a, b**). Thus, de-UFMylation frees 60S ribosomes from the ER-anchored E3^{UFM1}, releasing 60S subunits to the cytosol.

Conclusions

Our data reveal the elongated C-shaped structure of the heterotrimeric $E3^{UFM1}$ in a complex with 60S ribosomes. To our surprise, both our biochemical and structural data identified $E3^{UFM1}$ itself as the reader of its own 60S modification, resulting in stable 60S association and ATP-driven disruption of the SEC61-60S junction. Here, the UFM1 conjugate serves as the linchpin, coordinating $E3^{UFM1}$ binding via the DDRGK1 UFIM and concomitantly positioning the EBH of DDRGK1 such that it sterically clashes with (and therefore competes with) the trimeric SEC61 complex. The State 3 $E3^{UFM1}$-60S interaction is also incompatible with larger translocon assemblies, such as the SEC61-OST complex[25] for secreted glycoproteins and also the multi-pass membrane protein insertion SEC61-BOS-GEL complex[26–28]. The proposed SEC61-60S dissociation mechanism is likely to be multimodal and cooperative in a way that UFMylation not only stabilizes the DDRGK1 EBH at the tunnel exit, but also forces the ribosome to tilt with respect to the membrane to further destabilize the translocon connection (**Extended Data Fig. 9e, 9f**). We propose a model that explains the sequential engagement of $E3^{UFM1}$ with free 60S subunits which disrupts SEC61-binding and finally releases 60S subunits from the ER membrane upon deUFMylation (**Fig. 5c**). The presence of eIF6 (**Fig. 2b**) on these newly released 60S subunits suggests that they are now primed for recycling by SBDS and EFL1 to enter another round of translation initiation.

Our data identify $E3^{UFM1}$ as a likely candidate for the long-sought "detachment factor" first proposed by Günter Blobel in 1976 (ref. [29]) to explain the exceedingly slow rate of release of terminated 60S subunits from microsomal membranes observed upon translational termination in cell-free extracts[30]. There must also be UFM1-independent ways for post-termination 60S subunits to detach from ER translocons because mammalian cells can adapt to engineered deletion of UFM1 or its conjugation apparatus[2]. Moreover, some eukaryotic cells, most notably those comprising the

entire fungal kingdom, lack this Ubl and its conjugation system[31,32], despite being able to support rapid recycling of 60S subunits from the ER[33].

UFMylation-dependent weakening of the 60S-translocon junction was previously inferred from our investigation of the epistatic relationship between UFMylation and RQC machinery on ribosomes that stall during co-translational translocation of secretory proteins[4]. We propose that UFMylation, therefore, functions broadly to recycle translocon-engaged 60S subunits and translocons following either normal (**Fig. 5c**) or RQC-mediated termination. However, whether and how $E3^{UFM1}$ can engage ER-RQC derived 60S subunits with a bound peptidyl-tRNA, or even 80S ribosomes, remains to be elucidated.

Why have eukaryotic cells evolved such elaborate machinery to dissociate terminated 60S from the translocon? One possibility is that UFMylation prevents the initiation of non-secretory proteins on SEC61-docked 60S subunits by preventing eIF6 eviction. Normally, binding of eIF6 to the intersubunit interface of 60S subunits prevents 40S translation-initiation complexes from joining to form actively translating ribosomes. To license the large subunit to enter a new translation cycle, eIF6 must be evicted by the GTPase EFL1 and its cofactor SBDS[34]. Because $E3^{UFM1}$ sterically clashes with the EFL1/SBDS binding site on 60S subunits[35] (**Extended Data Fig. 2c**), persistent $E3^{UFM1}$ association ensures that post-termination 60S subunits at the ER cannot re-engage in translation until they are released from the ER by deUFMylation (**Fig. 5c**). While additional studies are clearly needed to understand how these steps are coordinated, the striking co-essential relationship of the UFM1 pathway with the 60S licensing factors EFL1/SBDS (**Extended Data Fig. 2a, b**) points to a fundamental, hitherto unappreciated role of this Ubl in orchestrating ribosome recycling and quality control.

REFERENCES

1. Cappadocia, L. & Lima, C. D. Ubiquitin-like Protein Conjugation: Structures, Chemistry, and Mechanism. *Chem. Rev.* **118**, 889–918 (2018).
2. Walczak, C. P. *et al.* Ribosomal protein RPL26 is the principal target of UFMylation. *Proc. Natl. Acad. Sci. U. S. A.* **116**, 1299–1308 (2019).
3. Wang, L. *et al.* UFMylation of RPL26 links translocation-associated quality control to endoplasmic reticulum protein homeostasis. *Cell Res.* **30**, 5–20 (2020).
4. Scavone, F., Gumbin, S. C., DaRosa, P. A. & Kopito, R. R. RPL26/uL24 UFMylation is essential for ribosome-associated quality control at the endoplasmic reticulum. *Proc. Natl. Acad. Sci. U. S. A.* (2023) doi:10.1073/pnas.2220340120.
5. Millrine, D., Peter, J. J. & Kulathu, Y. A guide to UFMylation, an emerging posttranslational modification. *FEBS J.* (2023) doi:10.1111/febs.16730.
6. Peter, J. J. *et al.* A non-canonical scaffold-type E3 ligase complex mediates protein UFMylation. *EMBO J.* **41**, e111015 (2022).
7. Ishimura, R. *et al.* Mechanistic insights into the roles of the UFM1 E3 ligase complex in ufmylation and ribosome-associated protein quality control. *Sci Adv* **9**, eadh3635 (2023).
8. Gerakis, Y., Quintero, M., Li, H. & Hetz, C. The UFMylation System in Proteostasis and Beyond. *Trends Cell Biol.* **29**, 974–986 (2019).
9. Xie, Z., Fang, Z. & Pan, Z. Ufl1/RCAD, a Ufm1 E3 ligase, has an intricate connection with ER stress. *Int. J. Biol. Macromol.* **135**, 760–767 (2019).
10. Branon, T. C. *et al.* Efficient proximity labeling in living cells and organisms with TurboID. *Nat. Biotechnol.* **36**, 880–887 (2018).
11. Kang, S. H. *et al.* Two novel ubiquitin-fold modifier 1 (Ufm1)-specific proteases, UfSP1 and UfSP2. *J. Biol. Chem.* **282**, 5256–5262 (2007).

12. Millrine, D. *et al.* Human UFSP1 is an active protease that regulates UFM1 maturation and UFMylation. *Cell Rep.* **40**, 111168 (2022).
13. Russell, D. W. & Spremulli, L. L. Mechanism of action of the wheat germ ribosome dissociation factor: interaction with the 60 S subunit. *Arch. Biochem. Biophys.* **201**, 518–526 (1980).
14. Gartmann, M. *et al.* Mechanism of eIF6-mediated inhibition of ribosomal subunit joining. *J. Biol. Chem.* **285**, 14848–14851 (2010).
15. Lyumkis, D. *et al.* Structural basis for translational surveillance by the large ribosomal subunit-associated protein quality control complex. *Proc. Natl. Acad. Sci. U. S. A.* **111**, 15981–15986 (2014).
16. Shao, S., Brown, A., Santhanam, B. & Hegde, R. S. Structure and assembly pathway of the ribosome quality control complex. *Mol. Cell* **57**, 433–444 (2015).
17. Shen, P. S. *et al.* Protein synthesis. Rqc2p and 60S ribosomal subunits mediate mRNA-independent elongation of nascent chains. *Science* **347**, 75–78 (2015).
18. Jumper, J. & Hassabis, D. Protein structure predictions to atomic accuracy with AlphaFold. *Nat. Methods* **19**, 11–12 (2022).
19. Evans, R. *et al.* Protein complex prediction with AlphaFold-Multimer. Preprint at https://doi.org/10.1101/2021.10.04.463034 (2022).
20. Halic, M. *et al.* Signal recognition particle receptor exposes the ribosomal translocon binding site. *Science* **312**, 745–747 (2006).
21. Beckmann, R. *et al.* Alignment of conduits for the nascent polypeptide chain in the ribosome-Sec61 complex. *Science* **278**, 2123–2126 (1997).
22. Habisov, S. *et al.* Structural and Functional Analysis of a Novel Interaction Motif within UFM1-activating Enzyme 5 (UBA5) Required for Binding to Ubiquitin-like Proteins and Ufmylation. *J. Biol. Chem.* **291**, 9025–9041 (2016).
23. Padala, P. *et al.* Novel insights into the interaction of UBA5 with UFM1 via a UFM1-interacting sequence. *Scientific Reports* vol. 7 Preprint at https://doi.org/10.1038/s41598-017-00610-0 (2017).
24. Martinez-Sanchez, A. *et al.* Template-free detection and classification of membrane-bound

complexes in cryo-electron tomograms. *Nat. Methods* **17**, 209–216 (2020).

25. Braunger, K. *et al.* Structural basis for coupling protein transport and N-glycosylation at the mammalian endoplasmic reticulum. *Science* **360**, 215–219 (2018).
26. McGilvray, P. T. *et al.* An ER translocon for multi-pass membrane protein biogenesis. *Elife* **9**, (2020).
27. Smalinskaitė, L., Kim, M. K., Lewis, A. J. O., Keenan, R. J. & Hegde, R. S. Mechanism of an intramembrane chaperone for multipass membrane proteins. *Nature* **611**, 161–166 (2022).
28. Sundaram, A. *et al.* Substrate-driven assembly of a translocon for multipass membrane proteins. *Nature* **611**, 167–172 (2022).
29. Blobel, G. Extraction from free ribosomes of a factor mediating ribosome detachment from rough microsomes. *Biochem. Biophys. Res. Commun.* **68**, 1–7 (1976).
30. Borgese, D., Blobel, G. & Sabatini, D. D. In vitro exchange of ribosomal subunits between free and membrane-bound ribosomes. *J. Mol. Biol.* **74**, 415–438 (1973).
31. Grau-Bové, X., Sebé-Pedrós, A. & Ruiz-Trillo, I. The eukaryotic ancestor had a complex ubiquitin signaling system of archaeal origin. *Mol. Biol. Evol.* **32**, 726–739 (2015).
32. Picchianti, L. *et al.* Shuffled ATG8 interacting motifs form an ancestral bridge between UFMylation and autophagy. *EMBO J.* **42**, e112053 (2023).
33. Jan, C. H., Williams, C. C. & Weissman, J. S. Principles of ER cotranslational translocation revealed by proximity-specific ribosome profiling. *Science* **346**, 1257521 (2014).
34. Jaako, P. *et al.* eIF6 rebinding dynamically couples ribosome maturation and translation. *Nat. Commun.* **13**, 1562 (2022).
35. Weis, F. *et al.* Mechanism of eIF6 release from the nascent 60S ribosomal subunit. *Nat. Struct. Mol. Biol.* **22**, 914–919 (2015).

MATERIALS AND METHODS

Plasmids

Plasmids and DNA constructs were generated using standard PCR and site directed mutagenesis techniques using Phusion polymerase (Thermo fisher) and/or Q5 High Fidelity polymerase (NEB) and verified by sequencing. Lentiviral vectors for the expression of DDRGK1, and UFL1 were generated from a modified pLVX vector[36] with an EF1a promoter and blasticidin selection marker. All lentivirus packaging vectors were obtained from Addgene. For cryo-EM pulldowns 3xFLAG N-terminally tagged UFM1 and C-terminally tagged UFL1 constructs were generated via PCR using Phusion polymerase (Thermo fisher) and inserted into modified pcDNA5/FRT/TO vectors harboring 3c cleavage sites.

Mammalian cell culture, lentivirus packaging, lentivirus infection, and cell line generation

K562 (myelogenous leukemia lymphoblast line, ATCC) were maintained in suspension between 2 x 10^5- and 1 x 10^6 cells/mL in RPMI media supplemented with 2 mM glutamine and 10 % FBS (Sigma-Aldrich). K562 cells stably expressing spCas9 were a gift from the Bassik Lab (Stanford University). HEK293 human embryonic kidney cells and HEK293T cells (ATCC) were grown and maintained in DMEM supplemented with 10 % FBS (Sigma-Aldrich). All cell lines were grown in humidified incubators at 37 °C in 5 % CO_2 and tested for mycoplasma bacteria by PCR using a kit from ABM Inc. with the manufacturer's instructions.

UFL1^{KO} HEK293 cells were generated via CRISPR knock-in of a stop cassette and puromycin resistance gene in a donor plasmid co-transfected with a px330 plasmid (Zhang Lab) carrying the sgRNA protospacer: CCAGCGGGCGCAGTTCGCCG. Cells were selected with puromycin starting ~3 days post transfection for ~ 5 days prior to single colony selection for clonal

knockout lines. UFL1 knockout was verified via western blot. N-terminal mini-Turbo[10] UFM1 knock-in cells were similarly generated in U2OS cells with wildtype, *UFSP2*^{KO}, or *UBA5*^{KO} (ref. [2]). A px330 plasmid with the protospacer sequence GAGCGGGAGAGAGTCAGGGT was co-transfected with a donor plasmid containing homology arms for UFM1 to insert the puromycin resistance gene followed by a P2A skip sequence and the mini-Turbo tag directly following the endogenous UFM1 start codon. Transfected cells were selected for puromycin resistance followed by clonal selection via limited dilution. Clonal lines with homozygous knock-in of the mini-Turbo tag were tested by western blots against UFM1 to ensure knock-in, competent conjugation to uL24 (for WT and *UFSP2*^{KO} backgrounds), and response to limited (200 nM) anisomycin treatments. Clones were further analyzed for a lack of core glycosylated CD147 stabilization[2] and mini-Turbo activity.

Lentivirus used to produce stable cell lines and K562 knockout lines was generated via transfection of HEK293T with second generation plasmids (pxPAX2, pMD2.G, and pLVX expression vector) or third generation plasmids (pRSV, pMDL, pVSVG, and pMCB320 sgRNA expression vectors) using *Trans*IT®-LT1 Transfection Reagent (Mirus) and the manufacturer's instructions and grown for 72 h before harvesting the viral supernatant. Supernatant (media) containing the viral particles was collected and filtered through a 0.45 µM syringe filter and frozen at -80 °C until use. Infections of K562 cells were performed via spin transduction; cells were resuspended in viral supernatant containing 8 µg/mL polybrene and centrifuged at 1000 x g for 2 h at 33 °C. Viral supernatant was removed and cells were resuspended in fresh RPMI (+ 10 % FBS) and grown for ~72 h before selection with puromycin for CRISPR mediated UFSP2 or UFM1 knockout lines. UFSP2 and UFM1 knockout K562 clonal lines were isolated via limited dilution. Stable UFL1-3xFLAG expressing HEK293 were generated via lentiviral transduction of

UFL1^{KO} cells (above) by the dilution of lentiviral supernatant into the media containing freshly trypsinized and plated cells (about 100,000) in the presence of 10 µg/mL polybrene. HEK293 were incubated with virus for 2-3 days prior to removing the viral supernatant and selection with blasticidin for stable UFL1-3xFLAG expressing cells.

HEK293 Flp-In TREx (Thermo fisher) cells were grown to 50 % confluency before transfection of 0.5 µg pcDNA5/FRT/TO vector containing N-terminally 3xFLAG tagged UFM1 or C-terminally 3xFLAG tagged UFL1 and 4.5 µg pOG44 (Thermo fisher) via 20 µg polyethyleneimine (PEI). 24 h following transfection, cells were split in 10 cm plates and selected via 10 µg/ml Blasticidin and 150 µg/ml Hygromycin B.

MiniTurbo-UFM1 sample preparation and mass spectrometry analysis

Five biological replicates of miniTurbo^{KI}-UFM1, and *UBA5*^{KO} miniTurbo^{KI}-UFM1 U2OS,and a single replicate of U2OS were prepared for miniTurbo-mediated proximity labeling experiments. Four 15 cm plates were grown for each replicate to 80-90 % confluency. Cells were treated with 50 µM of biotin for 4 h, removed from the 37 °C and washed 4 times with 15 mL ice cold 1X PBS, scraped from plates into 15 mL conical tubes, and spun at 800 x g for 5 min to pellet cells. Cells were lysed in 350 µL RIPA buffer (50 mM Tris pH 7.5, 150 mM NaCl, 0.5 % sodium deoxycholate, 0.1 % SDS, 1 % NP-40), incubated on ice for 15 min, and centrifuged at 21,000 x g for 10 min. Clarified supernatant (lysate) was transferred to a new 1.5 mL microcentrifuge tube and frozen in liquid nitrogen for future sample preparation. Samples were thawed in cool water and placed directly on ice, buffer-exchanged into RIPA buffer using PD10 columns (GE Healthcare) according to the manufacturer's instructions to reduce residual biotin. Biotinylated proteins were then processed as previously described[37]. In brief, lysate was normalized and 3.4 mg

was incubated with 30 µL pierce magnetic streptavidin beads (Thermo fisher, cat # 88816) pre-equilibrated in RIPA buffer overnight rotating at 4 °C. Using a magnetic microcentrifuge holder, RIPA buffer was removed, and beads were washed twice with 1 mL of RIPA buffer, twice with 1 mL of 2 % SDS in 50 mM HEPES, twice with 1 mL of 3 M Urea in 50 mM HEPES, once with 1 mL of 0.1 M sodium bicarbonate, two more times with 1 mL RIPA buffer, and twice with 1 mL of water. Captured protein was eluted from streptavidin beads by the addition of 100 µL of 1,1,1,3,3,3-Hexafluoro-2-propanol (HFIP; Millipore Sigma, Cat# 52517) and incubation at room temperature for 5 min while mixing. HFIP eluate was transferred to a new tube, and the process was repeated for a total of 200 µL of HFIP eluate. Samples were dried in a SpeedVac, and frozen dry for future processing. Samples were resuspended in 50 µl, 6 M Urea, 100 mM EPPS, pH 8.5. Trypsin (1 µg) was added to samples and the digest was incubated at 37 °C for 6 h. Biotinylated peptides were captured using streptavidin beads and supernatant was collected for downstream processing. Tandem mass tag (TMT) labeling of each sample was performed by adding 5 µL of the 20 ng/mL stock of TMT reagent along with acetonitrile to achieve a final acetonitrile concentration of approximately 30 % (v/v). Following incubation at room temperature for 1 h, the reaction was quenched with hydroxylamine to a final concentration of 0.5 % (v/v) for 15 min. The TMT-labeled samples were pooled together at a 1:1 ratio. The sample was vacuum centrifuged to near dryness and subjected to C18 solid-phase extraction (Sep-Pak, Waters). The sample was then fractionated according to manufacturer's instructions using High pH reversed-phase peptide fractionation kit (Thermo Fisher Scientific) for a final 6 fractions and subjected to C18 StageTip desalting prior to mass spectrometry analysis.

Mass spectrometry data were collected using an Orbitrap Fusion Lumos mass spectrometer (Thermo Fisher Scientific, San Jose, CA) coupled to a Proxeon EASY-nLC1200 liquid

chromatography (LC) pump (Thermo Fisher Scientific). Peptides were separated on a 100 µm inner diameter microcapillary column packed in house with ~35 cm of Accucore150 resin (2.6 µm, 150 Å, Thermo Fisher Scientific, San Jose, CA) with a gradient consisting of 5 %–15 % (0-70 min), 15 %–20 % (70-85 min) ACN-0.1 % FA over a total 95 min run at ~500 nL/min. For analysis, we loaded 1/3 of each fraction onto the column. Each analysis used the Multi-Notch MS^3-based TMT method[38], to reduce ion interference compared to MS^2 quantification[39], combined with the FAIMS Pro Interface (using previously optimized 3 CV parameters for TMT multiplexed samples[40] and combined with newly implemented Real Time Search analysis software[41,42]. The scan sequence began with an MS^1 spectrum (Orbitrap analysis; resolution 120,000 at 200 Th; mass range 400-1600 m/z; automatic gain control (AGC) target $8x10^5$; maximum injection time 100 ms). Precursors for MS^2 analysis were selected using a cycle type of 1.25 s/CV method (FAIMS CV =-40/-60/-80). MS^2 analysis consisted of collision-induced dissociation (quadrupole ion trap analysis; Rapid scan rate; AGC $1.0x10^4$; isolation window 0.7 Th; normalized collision energy (NCE) 35; maximum injection time 35 ms). Monoisotopic peak assignment was used, and previously interrogated precursors were excluded using a dynamic window (150 s ± 10ppm). Following acquisition of each MS^2 spectrum, a synchronous-precursor-selection (SPS) API-MS^3 scan was collected on the top 10 most intense ions b or y-ions matched by the online search algorithm in the associated MS^2 spectrum[41,42]. MS^3 precursors were fragmented by high energy collision-induced dissociation (HCD) and analyzed using the Orbitrap (NCE 65; AGC $2.5x10^5$; maximum injection time 300 ms, resolution was 50,000 at 200 Th).

Mass spectra were processed using a COMET-based in-house software pipeline. MS spectra were converted to mzXML using a modified version of ReAdW.exe. Database searching included all entries from the human UniProt database. This database was concatenated with one

554 composed of all protein sequences in the reversed order. Searches were performed using a 50 ppm
555 precursor ion tolerance and the product ion tolerance was set to 0.9 Da. Enzyme specificity was
556 assigned as trypsin. TMT tags on lysine residues and peptide N termini (+229.163 Da) and
557 carbamidomethylation of cysteine residues (+57.021 Da) were set as static modifications, while
558 oxidation of methionine residues (+15.995 Da) was set as a variable modification. Peptide-
559 spectrum matches (PSMs) were adjusted to a 1 % false discovery rate (FDR)[43,44]. PSM filtering
560 was performed using a linear discriminant analysis, as described previously[45], while considering
561 the following parameters: XCorr, peptide length, ΔCn, charge state, missed cleavages, and mass
562 accuracy of the precursor. TMT-based reporter ion quantitation, we extracted the summed signal-
563 to-noise (S:N) ratio for each TMT channel and found the closest matching centroid to the expected
564 mass of the TMT reporter ion (integration tolerance of 0.003 Da). Reporter ion intensities were
565 adjusted to correct for the isotopic impurities of the different TMT reagents according to
566 manufacturer specifications. Proteins were quantified by summing reporter ion signal-to-noise
567 measurements across all matching PSMs, yielding a ‘‘summed signal-to-noise’’ measurement.
568 PSMs with poor quality, MS^3 spectra with more than 5 TMT reporter ion channels missing, or
569 isolation specificity less than 0.7, or with TMT reporter summed signal-to-noise ratio that were
570 less than 140 or had no MS^3 spectra were excluded from quantification. Protein or peptide
571 quantification values were exported for further analysis in Microsoft Excel, and Perseus (version
572 1.5.3.2; ref. [46]). **SI Table 1** lists all quantified proteins as well as associated TMT reporter ratio to
573 control channels used for quantitative analysis. Annotations for endoplasmic reticulum protein
574 markers were assembled using the proteins which had scored with confidence ‘‘very high’’ or
575 ‘‘high’’ from a previously published HeLa dataset[47] and additional entries from manually curated
576 literature.

UFM1 pulldowns, sample processing and mass spectrometry

UFSP2/UFM1 double knock-out cells were transfected with UFM1 (a.a. 1-83; control) or SBP tagged UFM1 with a HC3 protease cleavage site and linker. 24 h after transfection cells were washed with PBS, harvested and lysed in a buffer containing 20 mM Tris pH 7.5, 100 mM NaCl, 10 mM $MgCl_2$, and 1% Decyl Maltose Neopentyl Glycol (DMNG) supplemented with EDTA-free Complete protease inhibitors (Roche), 0.5 mM TCEP, RNaseOUT (Thermo fisher), and 1 mM PMSF, on ice for 10 min. Lysate was clarified by centrifugation at 21,000 x g for 10 min at 4 °C three times. Clarified lysate was layered on top of 1 M sucrose cushion solution (20 mM Tris pH 7.5, 100 mM NaCl, 10 mM $MgCl_2$, and 1 % DMNG, and 1 M sucrose) for sucrose cushion sedimentation at 100,000 rpm in a TLA100.2 rotor at 4 °C for 1 h. The resulting pellet, containing crude ribosomes, was resuspended in lysis buffer after briefly washing the pellet with cold lysis buffer lacking DMNG. Resuspension was carried out by mechanically breaking the pellet and transferring it to a microcentrifuge tube using a pipette (P200), followed by mixing at 4 °C and additional mixing at 37 °C. Insoluble material was pelleted at 21,000 x g at 4 °C, and the supernatant was incubated with Dynabeads™ MyOne™ Streptavidin T1 beads pre-equilibrated in lysis buffer for 4 h at 4 °C rotating end-over-end. The flowthrough (unbound supernatant) was discarded and beads were washed 5 times with lysis buffer with low DMNG (0.02 %). Elution buffer (50 mM Tris pH ~7.5, 75 mM NaCl, 10 mM $MgCl_2$, 1 mM EGTA, and 30 mM biotin) was added to the beads and the mixture was mixed at 37 °C for 30 min to elute proteins. Eluate was processed via TCA precipitation for mass spectrometry analysis (below).

Proteins were extracted with 100 % TCA to a final volume of 25 % TCA and incubated overnight. The proteins were precipitated by centrifugation at 14,000 rpm for 10 min. TCA

precipitation was followed by three washes with 1 ml of ice-cold methanol. The precipitated pellet was dried in a speedvac and resuspended in 50 µL, 200 mM EPPS, pH 8.0. 0.5 µg of LysC (Wako cat. # 129-02541) and the sample was incubated at RT overnight while shaking. Then, 1 µg of Trypsin was added and the digest was incubated at 37 °C for 6 h. The sample was acidified and desalted by StageTip[48].

Mass spectrometry data were collected using a Exploris 480 mass spectrometer (Thermo Fisher Scientific, San Jose, CA) coupled with a Proxeon 1000 Liquid Chromatograph (Thermo Fisher Scientific). Peptides were separated on a 100 µm inner diameter microcapillary column packed with ~30 cm of Accucore C18 resin (2.6 µm, 150 Å, Thermo Fisher Scientific). We loaded ~1 µg onto the column.

Peptides were separated using a 1 h gradient of 0 to 28 % acetonitrile in 0.125 % formic acid with a flow rate of ~550 nL/min. The scan sequence began with an Orbitrap MS1 spectrum with the following parameters: resolution 60,000, scan range 350−1200 Th, automatic gain control (AGC) target 300 %, maximum injection time 25 ms, RF lens setting 40 %, and centroid spectrum data type. We selected the top twenty precursors for MS2 analysis which consisted of HCD high-energy collision dissociation with the following parameters: resolution 30,000, AGC was set at standard, maximum injection time 60 ms, isolation window 1.2 Th, normalized collision energy (NCE) 28, and centroid spectrum data type. In addition, unassigned and singly charged species were excluded from MS2 analysis and dynamic exclusion was set to 60 s.

Mass spectra were processed using a COMET-based in-house software pipeline. MS spectra were converted to mzXML using a modified version of ReAdW.exe. Database searching included all entries from the human UniProt database. This database was concatenated with one composed of all protein sequences in the reversed order. Searches were performed using a 50-ppm precursor ion tolerance and the product ion tolerance was set to 0.03 Da. Enzyme specificity was assigned as trypsin. Oxidation of methionine residues (+15.995 Da) was set as a variable modification. Peptide-spectrum matches (PSMs) were adjusted to a 1 % false discovery rate (FDR)[43,44]. PSM filtering was performed using a linear discriminant analysis, as described previously[45], while considering the following parameters: XCorr, peptide length, ΔCn, charge state, missed cleavages, and mass accuracy of the precursor. **Fig. 1c** displays proteins that have at least 5 spectral counts and is enriched at least 10-fold over the untagged UFM1 control pulldown. **SI Table 2** shows all proteins identified in this pulldown.

Cell Fractionation

Sequential detergent fractionations were performed as previously described[2]. Briefly, K562 cells were harvested, washed with PBS and resuspended in permeabilization buffer (0.02 % digitonin, 25 mM HEPES-KOH pH 7.5, 100 mM NaCl, and 10 mM $MgCl_2$) supplemented with EDTA-free Complete protease inhibitors (Roche), 0.5 mM TCEP, RNaseOUT (Thermo fisher), and phenylmethylsulfonyl fluoride (PMSF). Permeabilization was carried out for 5 min on ice before centrifugation for 5 min at 20,000 x g and 4°C. The resulting supernatant was collected as the cytosolic fraction. The pellet was briefly washed by gently resuspending in an equal volume of 25 mM HEPES-KOH pH 7.5, 100 mM NaCl, 10 mM NaCl and centrifugation at 8,000 x g for 5 min at 4 °C. The supernatant was discarded and the pellet was subsequently resuspended in an

equal volume of lysis buffer (25 mM HEPES-KOH pH 7.5, 100 mM NaCl, and 10 mM $MgCl_2$, and 0.5 % Triton X100 or 1 % DMNG for membrane polysome profiles and sucrose cushion sedimentation for E3-ribosome binding measurements), incubated for 5 min on ice, and centrifuged at 20,000 x g for 5 min at 4 °C. The resulting supernatant contained the membrane fraction. HEK293 cells were processed with the same protocol above, but with reduced digitonin (reduced to 0.015 %) in the initial permeabilization step.

Sucrose gradient sedimentation

K562 suspension cells were treated prior to polysome profiles: cells were collected into 15 mL falcon tubes on ice and supplemented with 200 µg/mL cycloheximide (CHX) at time of harvest. Cell suspensions were centrifuged at 800 x g for 5 min at 4 °C, resuspended in PBS containing 100 µg/mL CHX, and centrifuged again at 800 x g for 5 min to wash cells. Cells were then lysed on ice in polysome lysis buffer containing 25 mM HEPES-KOH pH 7.5, 100 mM NaCl, 0.5 mM TCEP, 10 mM $MgCl_2$, and 1% DMNG supplemented with EDTA-free Complete protease inhibitors (Roche), 0.5 mM TCEP, RNaseOUT (Thermo Fisher), and 1 mM PMSF. Lysate was mixed on ice for 10 min then spun to clarify at 21,000 x g for 10 min (at 4 °C) before layering onto a linear 10-50 % sucrose gradient (buffered with 25 mM HEPES-KOH pH 7.5, and containing 100 mM NaCl, and 10 mM $MgCl_2$, and 0.02 % DMNG). For polysome profiles of *in vitro* UFMylation reactions and purified ribosome subunits, the same 10-50 % gradients were generated in buffers lacking DMNG.

After samples were layered on gradients, centrifugation was carried out at 41,000 rpm in a SW41Ti rotor at 4 °C for 90 or 110 min and fractionated using a piston fractionator (Biocomp) affixed with a Triax UV detector and flow cell. Collected fractions were stored on ice or frozen

and stored at -80 °C until further processing. Sucrose gradient fractions were TCA (trichloro acetic acid) precipitated prior to analysis by immunoblot: sodium deoxycholate was added to each sample to a concentration of 0.02 % prior to precipitation with a final concentration of ice-cold TCA of 10 %. Samples were incubated at -20 °C for 1 h or overnight, protein was pelleted at 21,000 x g at 4 °C for 30 min, and washed with ice cold acetone, and centrifuged again at 21,000 x g at 4 °C for 30 min. The supernatant was removed, the protein pellet was dried at room temperature overnight and resuspended in 1X Laemmli sample buffer for immunoblot analysis.

E3^{UFM1}-ribosome co-sedimentation analysis

For UFL1-3xFLAG replacement lines, cells stably expressing C-terminally tagged 3xFLAG tagged UFL1 (and variants thereof) were grown to ~80 % confluency in 10 cm plates, washed 3 times with 5 mL of ice cold 1X PBS and harvested via scraping in 10 mL of 1X PBS. Cells were pelleted at 800 x g for 5 min at 4 °C and the supernatant was discarded. Cells were then resuspended in 0.5 mL of sucrose cushion lysis buffer (25 mM HEPES-KOH pH 7.5, 100 mM NaCl, 10 mM $MgCl_2$ and 1 % DMNG supplemented with 1 mM PMSF, 100 µg/mL cycloheximide (CHX), EDTA-Free Complete protease inhibitors (Roche), 0.5 mM TCEP, and RNAseOUT) incubated on ice for 10 min, and centrifuged for 10 min at 21,000 x g at 4 °C to clarify the lysate. The supernatant was collected and clarified again by centrifugation at 21,000 x g at 4 °C. Clarified lysate (400 µL) normalized for total protein concentration using a BCA assay was layered onto a sucrose cushion composed of 1 M sucrose, 25 mM HEPES-KOH pH 7.5, 100 mM NaCl, 10 mM $MgCl_2$ and 0.2 % DMNG, supplemented with 1 µg/mL cycloheximide, 0.5 mM TCEP, and centrifuged at 100,000 rpm in a TLA100.2 rotor for 1 h at 4 °C. The supernatant was removed and crude ribosome pellets were washed with 200 µL of sucrose cushion wash buffer (25 mM HEPES-

690 KOH pH 7.5, 100 mM NaCl, 10 mM $MgCl_2$) before resuspension in 1X Laemmli sample buffer
691 for immunoblot analysis.

692 *DDRGK1*^{KO} HEK293 were grown to ~80 % confluency in 6 well plates and transfected
693 with 2 µg pLVX plasmids containing C-terminally 3xFLAG tagged wildtype or mutant DDRGK1
694 with lipofectamine 3000 (ThermoFisher) according to the manufacturer's instructions. Cells were
695 split 24 h later into 2 wells of a six well plate and transfected again with 2 µg of DNA as above at
696 48 h post initial transfection. 20 h later, cells were washed 3 times with 2 mL of 1X PBS
697 supplemented with 100 µg/mL CHX, scraped and collected in 1 mL of 1X PBS (with 100 µg/mL
698 CHX), and pelleted at 500 x g for 5 min at 4 °C. For measurements of E3 association, cells were
699 treated with 200 nM anisomycin for 1 h to enhance the low-level E3-ribosome association in
700 HEK293 cells, lysed in 175 µL of sucrose cushion lysis buffer and pelleted as above using a
701 sucrose cushion of 250 µL in a TLA100.1 rotor with 150 µL of cell lysate. Crude ribosome pellets
702 were washed as above, but with 100 µL of wash buffer, and resuspended in 1X Laemmli sample
703 buffer for immunoblot analysis. Pelleting of E3associated ribosomes was performed three times
704 (biological triplicate) and the mean and standard deviations (error bars) are depicted in **Extended**
705 **Data Fig. 1l**.

706 For experiments in which wildtype or *DDRGK1*^{KO} HEK293 cells were fractionated prior
707 to sucrose pelleting, the cells suspended in PBS were split in equal volumes for whole cell (WC)
708 and fractionation samples prior to lysis. The WC cells were treated as above. Fractionated samples
709 were fractionated by sequential detergent extraction as described above. Equal volumes of each
710 fraction or WC lysate were layered on top of the 1 M sucrose cushion as above, pelleted and
711 analyzed by immunoblot analysis.
712

Ribosome-translocon association analysis

HEK293 WT, *UFC1*^{KO}, and *UFM1*^{KO} cells grown to ~80 % confluency in 6 well plates were treated with 5 µg/mL puromycin or 3.75 µM harringtonine for the indicated time points. Cells were washed once with 1 mL of ice cold 1X PBS and harvested by pipetting in 1.5 mL of 1X PBS. Cells from two wells were used for each condition. Cells were pelleted at 800 x g for 5 min at 4 °C and the supernatant was discarded. Cells were then resuspended in 0.5 mL of Triton lysis buffer (25 mM HEPES-KOH pH 7.5, 100 mM NaCl, 1 % Triton X100) supplemented with 1 mM PMSF, EDTA-Free Complete protease inhibitors (Roche), and 1 µM DTT, incubated on ice for 10 min, and centrifuged for 10 min at 21,000 x g at 4 °C to clarify the lysate. Clarified lysate (500 µL) normalized for total protein concentration using a BCA assay was layered onto a sucrose cushion composed of 1 M sucrose, 25 mM HEPES-KOH pH 7.5, 100 mM NaCl, with 1 mM PMSF, EDTA-Free Complete protease inhibitors (Roche), and 1 µM DTT, and centrifuged at 100,000 rpm in a TLA100.2 rotor for 1 h at 4 °C. The supernatant was removed and crude ribosome pellets were washed with 200 µL of ice cold H_2O, before resuspension in 1X Laemmli sample buffer for immunoblot analysis.

Preparation of salt-resistant 80S ribosomes

K562 cells at a density of ~1.5 x10^6 cells/mL were treated with 2 µg/mL harringtonine for 30 min. Cells were pelleted at 1000 x g for 5 min at 4 °C, resuspended in 35 mL of PBS (containing 100 µg/mL cycloheximide) and pelleted again at 1000 x g. The wash was repeated and the cells were lysed in 1 mL of a Triton lysis buffer (20 mM HEPES-KOH pH 7.5, 250 mM KCl, 15 mM $MgCl_2$, 1% Triton X100 supplemented with 1 mM PMSF, 0.5 mM TCEP, EDTA-free cOmplete protease inhibitors (Roche), and RNaseOUT) for 10 min on ice. Lysate was clarified at 8000 x g

for 10 min at 4 °C and layered onto a 10 – 50 % sucrose gradient and fractionated as above. Fractions containing the 80S ribosomes were pooled and pelleted via sucrose cushion sedimentation as described above in a TLA100.2 rotor. Pelleted 80S ribosomes were resuspended in 25 mM HEPES-KOH pH 7.5, 50 mM KCl, 15 mM $MgCl_2$, and 0.5 mM TCEP for *in vitro* UFMylation reactions.

In vitro UFMylation

In vitro UFMylation of ribosomes was performed as previously described[6]. Briefly, the purified UFMylation cascade was mixed and incubated with ribosomes with 1 µM UBA5, 1 µM UFC1, 2 µM UFM1, 100 nM UFL1/DDRGK1 complex, 200 nM CDK5RAP3, and 50 nM purified 60S ribosomes in 25 mM HEPES-KOH pH 7.5, 50 mM KCl, and 15 mM $MgCl_2$. A 100 mM stock of ATP was made fresh in 50 mM HEPES-KOH pH 7.5, pH adjusted to ~pH 7.0 with sodium bicarbonate, and added to a final concentration of 5 mM. Samples were then incubated at 35 °C for the indicated times and quenched by the addition of Laemmli sample buffer or placed on ice to halt the reaction before further analysis. Reactions performed on 60S in the presence of competing, salt-resistant 80S ribosomes were performed with a 2-fold molar excess of 80S over 60S ribosomes. *In vitro* UFMylation reactions used to prepare samples for Cryo-EM were performed similarly as above with 0.5 µM UBA5, 1 µM UFC1, 21 µM UFM1, 250 nM UFL1/DDRGK1 complex, 300 nM CDK5RAP3, and 200 nM purified 60S ribosomes in 25 mM HEPES-KOH pH 7.5, 50 mM KCl, and 10 mM $MgCl_2$ and 5 mM ATP and incubated for 15 min at 35 °C. UFMylated ribosomes were centrifuged at 21,000 x *g* for 5 min at 4 °C, and plunge frozen on Cryo-EM grids within ~1 h (see below).

Arrest peptide accumulation assay

Rescue experiments were performed by subjecting *DDRGK1*^{KO} HEK293 cells to two rounds of transfection with 2 µg of rescue plasmids (i.e., DDRGK1 WT, DDRGK1 UFIM^{mut}, DDRGK1 ΔEBM) for 72 h, similarly to the *DDRGK1*^{KO} rescues described above. The ribosome stalling reporter, SS^{VgV} (ref. [4]) (0.5 µg of plasmid DNA), was co-transfected with DDRGK1 rescue plasmids at the same time as the second DDRGK1 transfection (24 h prior to cell harvesting). Whole cell lysates were prepared in RIPA lysis buffer (50 mM Tris pH 7.6, 150 mM NaCl, 1 % NP-40, 0.5 % Sodium Deoxycholate, 0.1 % SDS) with protease inhibitor cocktail (cOmplete, EDTA-free Protease Inhibitor Cocktail; Roche) and 1 mM PMSF. Total protein concentration was determined for each sample with the Pierce BCA Protein Assay Kit (23225), and normalized samples were analyzed by SDS-PAGE and FLAG immunoblotting to detect arrest peptide (AP) produced by SS^{VgV}. Five biological replicates were performed; bar graphs in **Fig. 4i** show mean and standard deviation and significance determined using Dunnett's one-way ANOVA.

Protein purification

Mouse UFSP1 was purified as previously described[49] from a pet28a vector with a C-terminal His tag using a step gradient of imidazole to elute from Ni-NTA agarose (Qiagen) followed by dialysis and subsequent concentration to 100 µM in 20 mM HEPES (pH 7.5), 100 mm NaCl, and 2 mM dithiothreitol. Aliquots were frozen in liquid nitrogen and stored at -80 °C for future use. UFL1/DDRGK1, CDK5RAP3, UFC1, UBA5, and UFM1 were purified as previously described[6].

Affinity purification of UFM1 and UFL1-bound ribosomes for cryo-EM

HEK293 FlpIn TRex cells were grown to 50 % confluency and protein expression of 3xFLAG tagged UFM1 (FLAG-UFM1) or UFL1 (FLAG-UFL1) was induced via tetracyline (1 µg/ml). 22 h following induction, cells were harvested and washed twice with PBS via centrifugation at 127 x *g* for 10 min. Cells were then resuspended in lysis buffer (150 mM KOAc, 20 mM HEPES pH 7.5, 5 mM $MgCl_2$, 5 % glycerol, 3 % GDN, 1 mM DTT, 0.5 mM NaF, 0.1 mM Na_3VO_4, cOmplete EDTA free protease inhibitor (Roche)) and lysed via sonicating 4 x 10 s with 20 s on ice in between (Branson Sonifier 250). The lysate was clarified via centrifugation at 3,166 x *g* for 15 min and at 36,603 x *g* for 20 min then incubated with M2 anti-FLAG agarose beads (Sigma-Aldrich) on a rotating wheel for 120 min at 4 °C. Beads were washed twice with washing buffer (150 mM KOAc, 20 mM HEPES pH 7.5, 5 mM $MgCl_2$, 0.1 % GDN, 1 mM DTT, 0.5 mM NaF, 0.1 mM Na_3VO_4, cOmplete EDTA free protease inhibitor (Roche)), then once more using final buffer (150 mM KOAc, 20 mM HEPES pH 7.5, 5 mM $MgCl_2$, 1 mM DTT, 0.1 % GDN). Beads were transferred onto a 1 mL Mobicol (MoBiTec) and washed with 5 ml final buffer, then incubated with final buffer containing 40 µg 3C protease for 60 min at 4 °C. The eluate was collected via centrifugation and utilized further for single particle cryo-EM and NuPAGE gel electrophoresis.

3xFLAG-UFL1 purification was performed similarly, with a couple of differences. The lysis buffer was supplemented with 1 % digitonin instead of 3 % GDN, and, following elution with 3C protease, the ribosomes were pelleted through a sucrose cushion (20 mM HEPES pH 7.5, 150 mM KOAc, 5 mM $MgCl_2$, 0.1 % GDN, 1 M Sucrose) via centrifugation at 100,000 rpm for 1 h using a TLA 120.2 rotor, after which the pellet was resuspended in final buffer.

Electron microscopy and image processing

For the FLAG-UFM1 pulldown, 3.5 µl of sample was applied to Quantifoil R3/3 holey carbon grids with 2 nm continuous carbon coating, blotted for 3 s, then plunge frozen in liquid ethane using a Vitrobot Mark IV. Data collection was performed at 300 keV using a Titan Krios equipped with a K2 Summit direct electron detector using Smart EPU software versions 2.12.1 and 3.3.1 (Thermo Fisher) at a pixel size of 1.045 Å and a defocus range of -0.5 to -3.5 µm. Gain correction, alignment, and summation of movie frames was performed via MotionCor2 version 1.4.0 (ref. [50]) (1.16 e-/Å^2 dose per frame). Contrast transfer function (CTF) parameters were estimated using CTFFIND4 version 1.13 (ref. [51]) and GCTF (https://www2.mrc-lmb.cam.ac.uk/download/gctf/) [52]. The quality of the collected micrographs was assessed manually.

For the FLAG-UFM1 dataset, a total of 11,658 micrographs were selected. Particle picking was performed using crYOLO version 1.7.6 (ref. [53]) A total of 616,046 particles were picked, which then underwent two rounds of 2D classification in cryoSPARC version 3.2 (ref [54]). This yielded a total of 83,447 high-quality 60S particles and a minor subset of 80S particles (<10,000 particles). Brief analysis of the 80S subset revealed these to be previously published inactive ribosomes featuring eEF2-SERBP1 and EBP1 (ref. [55]) and were not processed further. The 60S was consensus refined in RELION (version 3.1.1; ref. [56]), followed by CTF refinement. 3D focused classification was performed using a soft mask focusing on the regions harboring non-ribosomal density for the E3^{UFM1} complex (spanning from the A, P and E sites down to uL24 and continuing further towards the ribosomal exit tunnel). This revealed one stable class consisting of 14,144 particles (16,9 % of all 60S particles) that was refined to an average resolution of 3.1 Å. A schematic representation of the refinement and particle sorting is provided in **Extended Data Fig. 3a**.

For the FLAG-UFL1 pulldown, 3.5 µl of sample was applied to Quantifoil R3/3 holey carbon grids with 2 nm continuous carbon coating, blotted for 3 s, then plunge frozen in liquid ethane using a Vitrobot Mark IV. Data collection was performed at 300 keV using a Titan Krios equipped with a SelectrisX Energy Filter and a Falcon4i direct electron detector at a pixel size of 0.727 Å and a defocus range of -0.5 to -3 µm and 60 e-/Å total dose. Gain correction, alignment, and summation of movie frames was performed via MotionCor2 (ref. [50]) with 20 EER frames grouped into one fraction, yielding 60 fractions with 1 e-/Å dose per fraction. Contrast transfer function (CTF) parameters were estimated using CTFFIND4 (ref. [51]) and GCTF[52].

A total of 50,993 micrographs were selected. Particle picking was performed in RELION 4.0.1 (ref. [57]), resulting in a total of 3,017,721 particles. 2D classification in RELION 4.0.1 using the VDAM algorithm yielded a total of 1,247,589 ribosomal particles. 3D classification with a soft mask around the 40S ribosomal subunit revealed a number of 60S classes with non-ribosomal density, as well as inactive 80S-eEF2-SERBP1/EBP1 complexes[55]. The 60S particles were further classified with a mask focusing around the A and P sites, which further revealed a small subpopulation of 60S corresponding to a biogenesis intermediate harboring LSG1, NMD3, and ZNF622 (ref. [58]). The remaining particles were sorted with a mask focusing around the tunnel exit. This revealed three major classes – one with SEC61 bound to the exit, another featuring the α-helix of DDRGK1 extending towards the tunnel exit, and a final one with EBP1 bound to the tunnel exit. The EBP1 population consisted of empty 60S subunits. The population featuring DDRGK1 was processed further with focused classification around the E3 complex used to sort out bad particles. This yielded a 3 Å final reconstruction corresponding to the entire E3 similar to the ones obtained from the 3xFLAG-UFM1 and in vitro datasets which was dubbed as State 3. For the SEC61-bound 60S, focused classification around H25ES7 and uL24 (around the expected

location of UFM1) revealed two states – one with UFL1 partially bound (referred to as State 1), and a second one with the E3 complex bound and uL24 modified, but with the α-helix of DDRGK1 delocalized (State 2). A final round of classification was done for State 1 in cryoSPARC (version 4.2) using 3D classification with a focused mask around SEC61. The final particles yielded a reconstruction of 3.27 Å. 3D variability analysis in cryoSPARC was used to sort out bad particles for State 2, and the final subset yielded a resolution of 3.33 Å. CTF refinements and final refinements of all states were performed with RELION 4.0.1. A schematic representation of the refinement and particle sorting is provided in **Extended Data Fig. 7**.

For *in vitro* UFMylated ribosomes, 2.5 µl of sample was applied to glow discharged copper 200 mesh R1.2/1.3 Ultrathin continuous carbon grids from Quantifoil, blotted for 3 s at 4 °C and 100 % humidity, and plunge frozen in liquid ethane using a Vitrobot Mark IV (Thermo fisher). Data collection was performed at the Stanford-SLAC Cryo-EM center (S^2C^2) on a Titan Krios G3i at 300 kV equipped with a K3 detector with a pixel size of 0.86 Å/pixel, a defocus range of -0.8 to -2.0 µm and a dose per frame of 0.8 $e^-/Å^2$. Gain correction, alignment, and summation of movie frames was performed via RELION 3.1.1's MotionCor implementation. CTF parameters were estimated using GCTF. A total of 10,692 micrographs were selected. 2D classification in cryoSPARC yielded 846,919 ribosomal particles. Focused classification in RELION 3.1.1 around the 40S subunit in order to separate 80S and 60S revealed a 60S class with non-ribosomal density (for the $E3^{UFM1}$ complex), 60S classes with and without E-site tRNA bound and two classes representing empty 80S ribosomes. For the first 60S class, using a soft mask focusing on regions where non-ribosomal extra density was observed, one stable class consisting of 35,935 particles (4.6 % of all particles) was isolated representing the stable 60S-UFM1-$E3^{UFM1}$ complex. This class

was refined to an average resolution of 2.9 Å. A schematic representation of the refinement and particle sorting is provided in **Extended Data Fig. 3b**.

All consensus refinement maps were post-processed using DeepEMhancer[59] and in some cases used for interpretation as indicated in the figure legends.

Model building and refinement

To generate a model for the 60S-UFM1-E3^{UFM1} complex in the best resolved state (obtained from the UFL1-pulldown State 3 complex), a model for the human 60S (derived from 80S, PDB code 6Z6M[55]) was used as a template. First, the 60S subunit was rigid-body fitted into the density maps using ChimeraX[60] with the exception of the L1 stalk, which adopted a different conformation in the 60S-UFM1-E3^{UFM1} complex. We therefore used the coordinates for the rRNA backbone of the L1 stalk from PDB code 8G5Y[61] as a starting point for modeling. Models for uL1 and eIF6 were used from the AlphaFold database (https://alphafold.ebi.ac.uk/) and real-space refined using Coot version 0.9.8 (ref. [62]). The model of the complex formed by UFM1, DDRGK1, CDK5RAP3 and the N-terminal region of UFL1 (1-389) was predicted using AlphaFold-Multimer[19] (see **Extended Data Fig. 5b**) and a model for the UFL1 C-terminal region (480-794) was derived from AlphaFold 2 prediction[18].

The model of the E3^{UFM1} complex was initially rigid-body fitted using the WH backbone of UFL1 and the GD2 and CC regions of CDK5RAP3 as a reference. The parts were then adjusted to fit into the density with Coot. For UFL1, the pWH and WH domains as well as parts of the CC regions could be fitted into the density map with high confidence, since a large number of aromatic and positively charged amino acid side chains were resolved well below 3.5 - 4 Å in the corresponding regions (see **Extended Data Fig. 4b** for local resolution). For the CTD of UFL1,

the local resolution of around 4 Å allowed to fit the peptide backbone, whereas the region linking the CTD and the CC (M522-G532) as well as the distal region of the CTD (E722-E794) displayed lower local resolution (above 4.5 Å) and was thus fitted as rigid body only. For the disordered region bipartite coiled-coil domain (CC) of UFL1, we identified density accounting for a small helix and loop (residues 416-448) referred to as the "PTC-loop", which was fitted *de novo*. The conformation of the PTC rRNA bases U4452 and A4548 (stacks with Y443 of UFL1) was adjusted to account for the remodeling due to the PTC loop. No or only weak density was present for the rest of the disordered loop as well as for the N-terminal helix of UFL1 (M1-Q25) and the C-terminal tail of UFM1, suggesting that these are flexible.

CDK5RAP3's GD2 and the adjacent parts of the CC helices were fitted by positioning several well-resolved bulky side chains. The overall local resolution in this region allowed for fitting a number of side chains with high confidence. The entire region below and adjacent to uL24, comprising UFM1, GD1 and adjacent CC helices of CDK5RAP3, displayed overall lower local resolution than the rest of the complex (between 4.5. and 7 Å) but still allowed clear assignment of secondary structure elements and thus rigid-body fitting of the respective AlphaFold models with only minor adjustments. The C-terminal pWH and WH domains of DDRGK1 were sufficiently resolved to fit bulkier side chains, particularly around the pWH interaction surface with UFL1's pWH. DDRGK1's linker region between the C-terminal domain and long helical region (residues 196-208, the so called UFM1-interacting motif or UFIM) and β2 (18-24) of UFM1 were predicted to have a particularly interesting interaction in the form of a β-augmentation. In addition, the first three turns N-terminal of the UFIM that terminate the long α-helix projecting towards the tunnel exit were also predicted to be in close vicinity to UFM1 and interact with it. This structural detail was in agreement with our density with respect to general positioning despite

the resolution being insufficient to verify interactions in molecular detail (see **Extended Data Fig. 6c**).

rRNA was partially remodeled in regions interacting with the E3 ligase (H69, H38 and H25ES7). Here, helices H69 and H38 could be fitted into the density map with high accuracy with the exception of the rRNA helix tips. While we omitted the helix tip of H69, the one of H38 was modeled based on PDB 8GLP[61] and was fit into our density where applicable. The conformation of H25ES7 is altered in the presence of E3 ligase, however. Here, resolution was insufficient for accurate modeling in State 3 (and State 2) and thus the model was trimmed. In addition, we trimmed other regions of the rRNA such as RNA loops and expansion segments where the density was insufficient to enable accurate model placement. The ribosomal protein uL13's C-terminal region was fitted into the State 3 structure up to the last discernible amino acid (R195). Finally, for uL1, most amino acid side chains were resolved, allowing to fit an AF2 model for uL1 with high confidence and refine it.

Models for partial 60S-E3^{UFM1}-SEC61 complexes as described for State 1 and State 2 were derived from the State 3 model. Unambiguous identification of SEC61 was supported by (i) the presence of a typical micelle directly under the tunnel exit, (ii) clear density at secondary structure resolution for the ribosome-interacting C-terminal portion of the SEC61α subunit and for the SEC61γ subunit and (iii) visualization of the SEC61α ribosome-binding loop 8-9 and loop 6-7 adjacent to the tunnel exit (**Extended Data Fig. 8**). A model for the trimeric complex from dog in the closed state (PDB 6W6L[26]) was rigid-body fitted into the respective densities. The local resolution of SEC61α loops 6-7 and 8-9 was sufficient for fitting some of the bulkier side chains **(Extended Data Fig. 8).**

Following rigid body fitting and real space refinement in Coot, the complete model was then refined with Phenix (version 1.12-4487) [63] and the Servalcat REFMAC5 pipeline[64]. Fine tuning of models (adjustment of rotamers, Ramachandran outliers and clashes) was performed using ISOLDE[65] in ChimeraX. At this point, we utilized the recently released model of the human 80S based on a 1.7 Å resolution map (PDB 8GLP[61]) to fine-tune the geometry of rRNA (phosphate-backbone conformation and sugar puckers) and ribosomal proteins of the core 80S ribosome. Model geometry was validated using Molprobity[66], and Phenix map to data cross correlation was utilized to evaluate overall density fits. As a final step, for UFM1, the E3 ligase, as well as SEC61, occupancy of regions with insufficient side chain information in the final maps was set to zero. Model and density figures were generated in ChimeraX version 1.6 (ref. [67,68]).

DeUFMylation of ribosomes with UFSP1

DeUFMylation of ribosomes in *UFSP2*^{KO} K562 lysate and *in vitro* UFMylated 60S ribosomes was performed with UFSP1 or UFSP1 inactivated by N-ethylmaleimide (NEM) as follows. UFSP1 was incubated with or without a final concentration of 20 mM NEM on ice for 20 min. Buffer was then exchanged into 20 mM HEPES-KOH pH 7.5, 100 mM NaCl, 10 mM $MgCl_2$, 1 mM TCEP using 0.5 mL Zeba 7 kDa (MWCO) 0.5 mL Desalting columns (Thermo Fisher, Cat# 89882) according to the manufacturer's instructions. Clonal *UFSP2*^{KO} K562 cells were harvested via centrifugation and washed twice with 10 mL of 1X PBS containing 100 µg/mL cycloheximide in a 15 mL falcon tube by centrifuging at 655 x g for 4 min at 4 °C. Cells were lysed in 20 mM HEPES-KOH pH 7.5, 100 mM NaCl, 10 mM $MgCl_2$, and 0.5 % Triton X100 containing 1 mM PMSF, 2X RNaseOUT, 0.5 mM TCEP, and 50 µg/mL cycloheximide for 10 min on ice, and clarified at 21,000 x g for 10 min at 4 °C. Lysate was then treated with 8 µM NEM-inactivated or

active UFSP1 for 10 or 20 min at 37 °C while mixing, placed on ice to slow deUFMylation and immediately layered onto a 10-50 % sucrose gradient for analysis by sucrose density sedimentation. A similar workflow was applied to *in vitro* prepared UFMylated ribosomes: UFMylated ribosomes were prepared as described above except that the reaction was quenched by addition of apyrase (Sigma Aldrich, Cat# A6237) at 5 U/mL and incubated on ice for 30 min. Active or inactivated UFSP1 was added to a final concentration of 8 µM and the sample was incubated at 37 °C for 20 min, placed on ice and immediately layered onto a 10-50 % sucrose gradient for sucrose gradient sedimentation.

Coessentiality network analysis

All essential UFMylation genes (UFM1, UFC1, UBA5, DDRGK1, UFL1, CDK5RAP3, ODR4 and UFSP1) were used as input for the FIREWORKS interactive network tool[69] (https://mendillolab.shinyapps.io/fireworks/). UFM1 co-dependencies were obtained from the Broad Institute's DEPMAP portal (https://depmap.org/portal/) (23Q4 release).

Antibodies

The following antibodies were used in this manuscript with the indicated dilutions: rabbit anti-UFM1, Abcam, Cat# ab109305, dilution, 1:1,000; mouse anti-UFSP2, Santa Cruz Biotechnology, Cat# sc-376084, dilution, 1:1,000; rabbit anti-UFC1, Abcam, Cat# ab189251, dilution, 1:2,000; rabbit anti-UBA5, Proteintech , Cat# 12093-1-AP, dilution, 1:2,000; rabbit anti-DDRGK1, Proteintech, Cat# 21445-1-AP, dilution, 1:1,000; rabbit anti-UFL1, Bethyl Laboratories, Cat# A303-456A, dilution, 1:2,000; rabbit anti-CDK5RAP3, Bethyl Laboratories, Cat# A300-870A, dilution, 1:2,000; rabbit anti-RPL26 (uL24), Abcam, Cat # ab59567, dilution, 1:3,000; mouse anti-RPL17 (C-8) (uL22), Santa Cruz Biotechnology, Cat# sc-515904, dilution, 1:2,000; rabbit anti-NEMF, Proteintech, Cat# 11840-1-AP, dilution, 1:2,000; rabbit anti-eIF6,

Bethyl Laboratories, Cat# A303-029A, dilution, 1:2,000; mouse anti-FLAG M2, Sigma-Aldrich Cat# F1804, dilution, 1:4,000; mouse anti-GAPDH clone D4C6R, Cell Signaling, 97166S, dilution, 1:5,000; rabbit anti-GAPDH clone 14C10, Cell Signaling, Cat# 2118, dilution, 1:5,000; IRDye 800CW Streptavidin, LI-COR Biosciences, Cat# 925-32230, dilution, 1:5,000; rabbit anti-SEC61β, Gift from Hegde Lab, dilution, 1:2,000; rabbit anti-SEC61α, Gift from Hegde Lab, dilution, 1:1,000; anti-Mouse IgG, IRDye 800CW, LI-COR Biosciences, Cat# 926-32210, RRID: AB_621842, dilution, 1:20,000; anti-Mouse IgG, IRDye 680LT, LI-COR Biosciences, Cat# 926-68020, RRID: AB_10706161, dilution, 1:20,000 ; anti-Rabbit IgG, IRDye 800CW, LI-COR Biosciences, Cat# 926-32211, RRID: AB_621843, dilution, 1:20,000; anti-Rabbit IgG, IRDye 680LT, LI-COR Biosciences, Cat# 926-68021, RRID: AB_10706309, dilution, 1:20,000. Antibodies were validated as described in the Reporting Summary.

Statistics and Reproducibility

All biochemical experiments, cell-based assays, and *in vitro* assays, in part or in whole, were successfully reproduced at least twice. For experiments in which statistics are given, details on the statistical analyses or tests are given in the methods pertaining to each experiment and/or the appropriate legend. Below is a description of experimental replications for each main and Extended Data figure.

For experiments with statistics given, the following list gives the p values for statistical tests given in the indicated figures and the number of biological replicates (n): in **Fig. 1a** p values are presented as the negative log of the p values. Values for each protein are given in Supplementary Table 1. In **Fig. 4e** comparing SEC61β intensities in ribosome pellets from WT and UFC1^{KO} cells treated with Puro to induce ribosome release from SEC61, p values were

1010 $1x10^{-4}$, $4x10^{-7}$, $2x10^{-5}$, and $1x10^{-9}$ for 1, 5, 15, and 30 min time points, respectively (n = 4). In
1011 **Fig. 4f** comparing SEC61β intensities in ribosome pellets from WT and $UFC1^{KO}$ cells treated
1012 with HT to induce ribosome release from SEC61, p values were $2x10^{-3}$, $4x10^{-5}$, and $3x10^{-2}$ for 5,
1013 15, and 30 min time points, respectively (n = 3). In **Fig. 4i** comparing ER-AP accumulation
1014 (signal) in $DDRGK1^{KO}$ cells rescued with WT DDRGK1 or empty vector, the p value was $7x10^{-4}$
1015 (n = 5). In **Extended Data Fig. 9d** comparing ribosome pellets of WT and $UFIM^{mt}$ rescued
1016 $DDRGK1^{KO}$ cells, p values were $7x10^{-3}$ and $2x10^{-5}$ for UFL1 signals and CDK5RAP3 signals,
1017 respectively (n = 3). In **Extended Data Fig. 9g** comparing SEC61α intensities in ribosome
1018 pellets from WT and $UFC1^{KO}$ cells treated with Puro to induce ribosome release from SEC61, p
1019 values were $1x10^{-2}$, $4x10^{-2}$, $6x10^{-2}$, $3x10^{-2}$ for 1, 5, 15, and 30 min time points, respectively (n =
1020 2). In **Extended Data Fig. 9h** comparing SEC61α intensities in ribosome pellets from WT and
1021 $UFC1^{KO}$ cells treated with HT to induce ribosome release from SEC61, p values were $3x10^{-4}$,
1022 $2x10^{-5}$, and $7x10^{-5}$ for 5, 15, and 30 min time points, respectively (n = 3). In **Extended Data Fig.**
1023 **9i** comparing SEC61β intensities in ribosome pellets from WT and $UFM1^{KO}$ cells treated with
1024 HT to induce ribosome release from SEC61, p values were $5x10^{-3}$, $1x10^{-2}$, and $2x10^{-3}$ for 5, 15,
1025 and 30 min time points, respectively (n = 3). **Extended Data Fig. 9i** comparing SEC61α
1026 intensities in ribosome pellets from WT and $UFM1^{KO}$ cells treated with HT to induce ribosome
1027 release from SEC61, p values were $3x10^{-2}$, $1x10^{-2}$, and $1x10^{-3}$ for 5, 15, and 30 min time points,
1028 respectively (n = 3). The number of biological replicates for these experiments was chosen based
1029 on the effect size of the measurement and/or the expected variability or, in the case of **Fig. 1a**,
1030 the available TMT channels to maximize statistical robustness. All experimental data were
1031 included in the statistics; no replicates were excluded from the analyses.

The following details the robustness of experimental data for which no statistical analysis was performed: For the experiment in **Fig. 1b and c**, while this experiment as it is presented was performed only once under these exact conditions, other very similar experiments were performed to test a number of the proteins seen in the identification list by western blot and was replicated in a similar mass spectrometry (MS) experiment (albeit with a different solubilizing detergent) which gave similar results. Furthermore, experiments in **Fig. 1d and e, Extended Data Fig. 1k, i, m and n** replicate the binding of the $E3^{UFM1}$ and this is underscored by the Cryo-EM from cell pulldowns using FLAG-UFM1 maps and models. Mass spectrometry of these FLAG-UFM1 Cryo-EM samples, revealed similar results as **Fig. 1c,** but these data did not have a background control to exclude nonspecific proteins. Hence, the pulldown MS experiment in **Fig. 1c** and its findings can be considered replicated. The experiments in **Fig. 1d** were replicated in different parts during pilot experiments and during method optimization, and in different cell lines (HEK293 and/or U2OS with WT, $UFSP2^{KO}$ and/or $UFM1^{KO}$ cells) with no fewer than two observations of each protein probed in these extremely similar experiments. All results were very similar. The experiments in **Fig. 1e** and the related experiments performed in **Extended Data Fig. 1m and n** were performed twice, albeit with slightly different parameters (e.g. for sucrose sedimentation conditions) and in highly similar experiments during the optimization of conditions. **Extended Data Fig. 1b, d, and c** were replicated multiple times in part or in whole during the development of the miniTurbo mass spectrometry experiments with each observation being made at least twice. These observations are also made in the mass spectrometry data in **Fig. 1a** and were also observed in other mass spectrometry experiments not in this manuscript with statistical analyses and at least four replicates (i.e. such is the case for **Extended Fig. 1d and c**). Each part of the experiment in **Extended Fig. 1e** was replicated extensively, with two

replications of the eL36-SBP pulldown being performed and > 5 replicates being performed for SBP-UFM1 pulldowns during mass spectrometry sample optimization and early Cryo-EM sample preparations. The qualitative observations in **Extended Data Fig. 1g** was replicated in K562 cells (as depicted) under very similar conditions, and replicated in part or in whole in HEK293 and U2OS cell lines. These observations are also present in **Fig. 1d**, but with much better detection of modified uL22 after membrane ribosome extraction. The densitometry values of plots from **Extended Data Fig. 1 g and h** are available as source data in Supplemental Table 3. **Extended Data Fig. 1k and i** were performed with biological triplicates as shown; while the mean and SD are shown, a statistical test was not performed for these data. The data presented in **Extended Data Fig. i and j** are controls that only pertain to the experimental validity of the experiments in **Fig. 1d** and illustrate the purity of fractions used for those specific samples. The experiments performed in **Fig. 2a** and **Fig. 4a** pertain to specific samples as well; nonetheless these pulldowns and gels were replicated twice with very similar conditions during different cryo-EM sample preparations. The data presented in **Fig. 4c** was replicated in whole twice. The experiment in **Fig. 4d** was replicated in part or in whole during multiple pilot experiments with each observation made at least twice. The experiments in **Fig. 5a and b** were replicated twice with very similar experimental procedures; panels **Fig. 5a and b** are also highly complementary experiments. Hence, all experiments can be considered replicated at least twice.

Uncropped images, including replicate gels used in statistics, and densitometry data for all plots generated in the manuscript are available as source data in Supplementary Figures 1-6 and in Supplementary Tables 1-9, respectively. For more details see the SI Guide of this manuscript. GraphPad Prism Version 10.1.0 was used for all plots made and statistics generated for immunoblot data. Densitometry was performed in Image Studio Lite Version 5.2.5.

Cryo-EM data collections from FLAG-UFL1-pulldowns similar to the one shown in **Fig. 4a** were performed twice but only the latter was used for this study. For the first dataset 9907 micrographs were collected yielding a total of 104,395 ribosomal particles. 2D and 3D Classification of those particles resulted in similar particle ensembles as presented in this paper, including States 1, 2, and 3 of the 60S-UFM1-E3^{UFM1} complex. For the second dataset 50,993 micrographs were selected, yielding 1,247,589 ribosomal particles. This dataset largely reproduced the first dataset, but with more detail due to the higher number of particles and this better resolution for each relevant class.

Cryo-EM data from the FLAG-UFM1-pulldown (**Fig. 2a**) and the *in vitro* reconstituted 60S-UFM1-E3^{UFM1} complex were only collected once. Yet, all datasets were processed with both RELION and CryoSPARC, respectively, always reproducing essentially the same results.

Data Availability

All relevant data are included in the manuscript and Supplementary Information. Mass spectrometry data files have been uploaded to the MassIVE proteomics database MSV000093510 (ftp://massive.ucsd.edu/MSV000093510/).

The cryo-EM structural data generated in this study have been deposited in the Protein Data Bank and the Electron Microscopy Data Bank under accession codes EMD-16903 for the 60S-UFM1-E3^{UFM1} (obtained from the UFM1 pulldown), EMD-16908 and PDB-8OJ8 for the 60S-E3^{UFM1}-SEC61 complex in State 1, EMD-16902 and PDB-8OJ0 for the 60S-UFM1-E3^{UFM1}-SEC61 complex in State 2, EMD-16880 and PDB-8OHD for the 60S-UFM1-E3^{UFM1} complex in State 3 (States 1, 2 and 3 obtained from the UFL1 pulldown) and EMD-16905 and PDB-8OJ5 for the *in vitro* reconstituted 60S-UFM1-E3^{UFM1} complex (State 3). The structures used for

atomic model building of 60S-UFM1-E3^{UFM1} and 60S-UFM1-E3^{UFM1}-SEC61 complexes are available in Worldwide Protein Data Bank (wwPDB) with accession code 8GLP [https://www.wwpdb.org/pdb?id=pdb_00008glp], 8G5Y [https://www.wwpdb.org/pdb?id=pdb_00008g5y], 6Z6M [https://www.wwpdb.org/pdb?id=pdb_00006z6m] and 6W6L [https://www.wwpdb.org/pdb?id=pdb_00006w6l]

Additional References

36. Leto, D. E. *et al.* Genome-wide CRISPR Analysis Identifies Substrate-Specific Conjugation Modules in ER-Associated Degradation. *Mol. Cell* **73**, 377–389.e11 (2019).

37. An, H., Ordureau, A., Körner, M., Paulo, J. A. & Harper, J. W. Systematic quantitative analysis of ribosome inventory during nutrient stress. *Nature* **583**, 303–309 (2020).

38. McAlister, G. C. *et al.* Increasing the multiplexing capacity of TMTs using reporter ion isotopologues with isobaric masses. *Anal. Chem.* **84**, 7469–7478 (2012).

39. Paulo, J. A., O'Connell, J. D. & Gygi, S. P. A Triple Knockout (TKO) Proteomics Standard for Diagnosing Ion Interference in Isobaric Labeling Experiments. *J. Am. Soc. Mass Spectrom.* **27**, 1620–1625 (2016).

40. Schweppe, D. K. *et al.* Characterization and Optimization of Multiplexed Quantitative Analyses Using High-Field Asymmetric-Waveform Ion Mobility Mass Spectrometry. *Anal. Chem.* **91**, 4010–4016 (2019).

41. Erickson, B. K. *et al.* Active Instrument Engagement Combined with a Real-Time Database Search for Improved Performance of Sample Multiplexing Workflows. *J. Proteome Res.* **18**, 1299–1306 (2019).

42. Schweppe, D. K. *et al.* Full-Featured, Real-Time Database Searching Platform Enables Fast and Accurate Multiplexed Quantitative Proteomics. *J. Proteome Res.* **19**, 2026–2034 (2020).

43. Elias, J. E. & Gygi, S. P. Target-decoy search strategy for increased confidence in large-scale protein identifications by mass spectrometry. *Nat. Methods* **4**, 207–214 (2007).

44. Elias, J. E. & Gygi, S. P. Target-Decoy Search Strategy for Mass Spectrometry-Based Proteomics. *Methods in Molecular Biology* 55–71 Preprint at https://doi.org/10.1007/978-1-60761-444-9_5 (2010).

45. Huttlin, E. L. *et al.* A tissue-specific atlas of mouse protein phosphorylation and expression. *Cell* **143**, 1174–1189 (2010).

46. Tyanova, S. *et al.* The Perseus computational platform for comprehensive analysis of

(prote)omics data. *Nat. Methods* **13**, 731–740 (2016).

47. Itzhak, D. N., Tyanova, S., Cox, J. & Borner, G. H. Global, quantitative and dynamic mapping of protein subcellular localization. *Elife* **5**, (2016).

48. Ishihama, Y., Rappsilber, J. & Mann, M. Modular stop and go extraction tips with stacked disks for parallel and multidimensional Peptide fractionation in proteomics. *J. Proteome Res.* **5**, 988–994 (2006).

49. Ha, B. H. *et al.* Structural basis for Ufm1 processing by UfSP1. *J. Biol. Chem.* **283**, 14893–14900 (2008).

50. Zheng, S. Q. *et al.* MotionCor2: anisotropic correction of beam-induced motion for improved cryo-electron microscopy. *Nat. Methods* **14**, 331–332 (2017).

51. Rohou, A. & Grigorieff, N. CTFFIND4: Fast and accurate defocus estimation from electron micrographs. *J. Struct. Biol.* **192**, 216–221 (2015).

52. Zhang, K. Gctf: Real-time CTF determination and correction. *J. Struct. Biol.* **193**, 1–12 (2016).

53. Wagner, T. *et al.* SPHIRE-crYOLO is a fast and accurate fully automated particle picker for cryo-EM. *Commun Biol* **2**, 218 (2019).

54. Punjani, A., Rubinstein, J. L., Fleet, D. J. & Brubaker, M. A. cryoSPARC: algorithms for rapid unsupervised cryo-EM structure determination. *Nat. Methods* **14**, 290–296 (2017).

55. Wells, J. N. *et al.* Structure and function of yeast Lso2 and human CCDC124 bound to hibernating ribosomes. *PLoS Biol.* **18**, e3000780 (2020).

56. Zivanov, J. *et al.* New tools for automated high-resolution cryo-EM structure determination in RELION-3. *Elife* **7**, (2018).

57. Kimanius, D., Dong, L., Sharov, G., Nakane, T. & Scheres, S. H. W. New tools for automated cryo-EM single-particle analysis in RELION-4.0. *Biochem. J* **478**, 4169–4185 (2021).

58. Liang, X. *et al.* Structural snapshots of human pre-60S ribosomal particles before and after nuclear export. *Nat. Commun.* **11**, 3542 (2020).

59. Sanchez-Garcia, R. *et al.* DeepEMhancer: a deep learning solution for cryo-EM volume post-

processing. *Commun Biol* **4**, 874 (2021).

60. Pettersen, E. F. *et al.* UCSF ChimeraX: Structure visualization for researchers, educators, and developers. *Protein Sci.* **30**, 70–82 (2021).

61. Holm, M. *et al.* mRNA decoding in human is kinetically and structurally distinct from bacteria. *Nature* **617**, 200–207 (2023).

62. Emsley, P. & Cowtan, K. Coot: model-building tools for molecular graphics. *Acta Crystallogr. D Biol. Crystallogr.* **60**, 2126–2132 (2004).

63. Liebschner, D. *et al.* Macromolecular structure determination using X-rays, neutrons and electrons: recent developments in Phenix. *Acta Crystallogr D Struct Biol* **75**, 861–877 (2019).

64. Yamashita, K., Palmer, C. M., Burnley, T. & Murshudov, G. N. Cryo-EM single-particle structure refinement and map calculation using Servalcat. *Acta Crystallogr D Struct Biol* **77**, 1282–1291 (2021).

65. Croll, T. I. ISOLDE: a physically realistic environment for model building into low-resolution electron-density maps. *Acta Crystallogr D Struct Biol* **74**, 519–530 (2018).

66. Williams, C. J. *et al.* MolProbity: More and better reference data for improved all-atom structure validation. *Protein Sci.* **27**, 293–315 (2018).

67. Goddard, T. D. *et al.* UCSF ChimeraX: Meeting modern challenges in visualization and analysis. *Protein Sci.* **27**, 14–25 (2018).

68. Pettersen, E. F. *et al.* UCSF ChimeraX: Structure visualization for researchers, educators, and developers. *Protein Sci.* **30**, 70–82 (2021).

69. Amici, D. R. *et al.* FIREWORKS: a bottom-up approach to integrative coessentiality network analysis. *Life Sci Alliance* **4**, (2021).

Acknowledgements

We thank C. Ungewickell, S. Rieder, and Andrea Gilmozzi for excellent technical assistance, M.C. Riepe for helpful discussion throughout this work and for critical reading of the manuscript, and A. Ting for reagents and advice with the proximity labeling experiments. This study was supported by grants from ERC (RELYUBL, 677623), the Lister Institute of Preventive Medicine, BBSRC (BB/T008172/1) and MRC (grant MC_UU_00018/3) to Y. Kulathu; from ERC (ADG 885711 Human-Ribogenesis and DFG (SFB/TRR-174, BE1814/15-1, BE1814/1-1) to R. Beckmann; and from the NIH to R.R. Kopito (1R01GM148477, 5R01GM074874), J.W. Harper (RO1AG011085, R01NS083524), and J.A. Paulo (K01DK098285). P.A. DaRosa was supported by NIH training grant 5T32NS007280. S.C. Gumbin was supported by NIH training grant T32GM007276 and by the Stanford Graduate Fellowship.

Some of this work was performed at the Stanford-SLAC Cryo-EM Center (S2C2), which is supported by the National Institutes of Health Common Fund Transformative High-Resolution Cryo-Electron Microscopy program (U24 GM129541). The content is solely the responsibility of the authors and does not necessarily represent the official views of the National Institutes of Health. The authors would also like to thank the following S2C2 personnel for their invaluable support and assistance: Yan Liu.

Author Contributions

P.A.D., I.P., R.R.K, T.B., and R.B. conceived and designed the project. P.A.D. devised and performed all cell-based and cell-free biochemical experiments, except the translocon release assays, which were designed and performed by S.C.G and M.W., and the arrest peptide accumulation assay, performed by F.S. P.A.D. prepared the cryo-EM grids for the *in vitro*

UFMylated 60S samples. P.A.D., A.O., J.A.P and J.W.H. conceived and designed the proximity labeling and affinity capture experiments and A.O., J.A.P performed the mass spectrometry experiments. J.J.P and Y.K. provided purified UFMylation enzymes and assisted with *in vitro* UFMylation. I.P. generated FLAG-UFM1 and FLAG-UFL1 constructs and cell lines, performed immunoisolation, and processed all the cryo-EM data. P.A.D. and I.P. conducted and analyzed the AlphaFold modeling. I.P. generated molecular models and, together with T.B. and R.B. analyzed the $E3^{UFM1}$ structures. P.A.D., I.P., R.R.K, T.B., and R.B. wrote and edited the manuscript with input from all authors.

Competing interest declaration

All authors declare that they have no conflicts of interest.

Additional information

Supplementary Information is available for this paper.

Correspondence and requests for materials should be addressed to Ron R Kopito (kopito@stanford.edu) and Roland Beckmann (beckmann@genzentrum.lmu.de).

FIGURE LEGENDS

Fig. 1: $E3^{UFM1}$ forms a long-lived complex with UFMylated 60S

a, Volcano plot for proteins proximal to UFM1 conjugates identified by TMT-MS3 in wildtype vs. *UBA5*^{KO} U2OS cells. UFM1 conjugates are highly enriched in ER membrane components, particularly those associated with protein translocation/insertion and UFM1 conjugation. Grey area denotes statistically significant boundaries (two-tailed Student's t-test [S0 = 0.585], corrected for multiple comparisons by permutation-based false discovery rate [FDR] [1%]). **b, c**, Experimental workflow (**b**) and table (**c**) summarizing MS/MS analysis of affinity-captured UFMylated ribosomes. $E3^{UFM1}$ subunits (red), 60S biogenesis/recycling factors (green), and ER membrane translocation machinery (blue). Table shows proteins that were enriched by > 10-fold over control and had at least 4 spectral counts. **d**, Sucrose gradient sedimentation analysis of membrane fractions from K562 cells of the indicated genotypes immunoblotted with the indicated antibodies. **e**, Sucrose gradient sedimentation analysis of purified 60S, UFMylated by purified UFMylation components (E1, E2, E3, and UFM1) *in vitro* in the presence or absence of ATP as indicated. **f**, 60S is the preferred substrate of UFMylation. Purified 60S or salt-washed 80S ribosomes were incubated for the indicated times with purified UFMylation components, fractionated on sucrose gradients, and analyzed by immunoblotting for uL24. Blots and MS experiments are representative of at least two independent replicates with very similar results (see "Reproducibility and statistics" section of Methods for details). Source data is available in Supplementary Tables 1 and 2 (for **a** and **c**) and Supplementary Fig. 1 (for **d**-**f**).

Fig. 2: Structural analysis of the 60S-UFM1-$E3^{UFM1}$ complex

a, Coomassie stained Nu-PAGE gel of 3x-FLAG-UFM1 pulldown showing enrichment of E3^{UFM1} subunits. **b**, Cryo-EM density map of the native 60S-UFM1-E3^{UFM1} complex (native) isolated from cells shown from the intersubunit interface side as "crown view". CP, central protuberance. Non-ribosomal extra density for 60S-UFM1-E3^{UFM1} spans from the tunnel exit, over uL24, towards the L1 stalk, and over the tRNA binding sites. **c**-**e**, Cryo-EM density map of 60S-UFM1-E3^{UFM1} complex reconstituted with purified components (*in vitro*) shown (**c**) at the same angle as in (**b**), as back view (**d**; rotated ~180° from (**b**)) and as bottom view (**e**; rotated ~90° from (**d**)) near tunnel exit (Exit; red dashed circle). *In vitro* map recapitulates the densities seen from cellular pulldowns. **f**, Positions of A- P- and E-sites with tRNAs superimposed to a model for the 60S subunit shown at the same angle as densities in (**b**) and (**c**). rRNA, dark gray; ribosomal-proteins, light gray. PDB codes: 6z6m for E-tRNA, 5mc6 for A- and P-tRNAs and 60S. **g**, Molecular model of the 60S-UFM1-E3^{UFM1} complex derived from density in (**c**). All cryo-EM maps are shown after post-processing with DeepEMhancer software. For clarity, the density for the E3^{UFM1} complex is shown at lower contour levels as compared to the 60S. Source data is available in Supplementary Fig. 1 (for **a**).

Fig. 3: Organization of the E3^{UFM1} complex bound to UFMylated 60S

a, Schematic representation of the E3^{UFM1} complex domain organization and interactions among the components of the E3 complex, UFM1, and the 60S subunit. **b**, Overview of the 60S-bound UFM1-E3^{UFM1} molecular model describing the architecture of the 60S-bound UFM1-E3^{UFM1}. **c**, Position of the UFL1 CTD between H38 and H69 with positively charged residues close to the rRNA highlighted in blue. **d**, Position of the DDRGK1 exit-binding α-helix (EBH) close to the tunnel exit; the UFMylation target lysine on uL24, K134, and

positively charged residues at the tip of the DDRGK1 exit-binding motif (EBM) are highlighted green and blue, respectively. **e**, Interaction of DDRGK1 and CDK5RAP3 with UFM1. Left, predicted β-augmentation of the UFIM-motif and the preceding three turns of the exit-binding α-helix of DDRGK1 with UFM1. Right, alternate view showing proximity and limited interactions with CDK5RAP3. **f**, Structured PTC-loop of UFL1 (D416-V448) near the peptidyl transferase center (PTC) within the disordered region (UFL1 N391-F479). In (**b-d**), thumbnails indicate the overall complex orientation.

Fig. 4: Sequential E3^{UFM1} binding and UFMylation of 60S promotes SEC61 displacement

a, Coomassie-stained NuPAGE gel of 3xFLAG-UFL1 pulldown. **b**, Cryo-EM models of 60S-E3^{UFM1} states from 3xFLAG-UFL1 pulldown. **c,** Immunoblot analysis of WT or *UFL1*^{KO} HEK293 cells expressing 3X-FLAG-tagged full-length (FL) or C-terminally truncated UFL1 mutants, immunoblotted for the indicated proteins. **d**, Immunoblot analysis of ribosome pellets or inputs from whole cell lysates ("WC") or cytosolic ("C") and membrane ("M") fractions derived from *DDRGK1*^{KO} HEK293 cells expressing WT DDRGK1, UFIM^{mt}, or ΔEBM mutants. **e, f,** Dissociation of 60S from the translocon following puromycin-induced (**e**) or run-off (**f**) translation termination in *UFC1*^{KO} cells. Top, immunoblot analysis of ribosome pellets or inputs from WT or *UFC1*^{KO} HEK293 cells treated with indicated drugs. Asterisk in **f**, nonspecific band. Bottom, quantification of SEC61β band intensities in ribosome pellets. Data show mean ± SD and p values relative to untreated from indicated comparisons derived from two-way ANOVA followed by uncorrected Fisher's LSD tests, $n = 4$ (**e**) and $n = 3$ (**f**) biological replicates. **g**, Restricted

access of LTN1 to glycosylated, FLAG-tagged arrest peptide (ER-AP) on SEC61-docked 60S generated from splitting stalled ER-ribosomes. **h**, Rescue of ER-AP degradation in *DDRGK1*^{KO} cells transfected with WT, but not mutant (UFIM^{mt} and ΔEBM) DDRGK1. **i**, Quantification of ER-AP intensities from data as in (**h**). Data show mean GAPDH-normalized fold-change ± SD relative to unrescued *DDRGK1*^{KO} cells and p value from indicated comparison derived from one-way ANOVA of $n = 5$ biological replicates. Source data is available in Supplementary Fig. 2 (for **a** and **c**-**e**), Supplementary Fig. 3 (for **f**, and **h**), and Supplementary Tables 6, 7, and 9 (for **e**, **f**, and **i**, respectively). For p values and data replication descriptions see "Reproducibility and Statistics" section of the Methods.

Fig. 5: De-UFMylation promotes dissociation of 60S and E3^{UFM1}

a, Lysates of *UFSP2*^{KO} K562 cells were treated with active (black) or NEM-inactivated (red) murine UFSP1 (mUFSP1) and subjected to sucrose density gradient sedimentation fractionation (top) followed by immunoblotting with the indicated antibodies (bottom). **b**, Purified 60S was UFMylated *in vitro* with purified components and treated with recombinant mUFSP1 and analyzed as in (**a**). Data in a and b were replicated at least twice in independent experiments with similar results (for details see "Reproducibility and Statistics" section of Methods). Source data is available in Supplementary Fig. 4. **c**, Model for sequential interaction of SEC61-bound 60S with E3^{UFM1}.

EXTENDED DATA FIGURE LEGENDS

Extended Data Fig. 1: E3^{UFM1} selectively modifies and then binds 60S ribosomes.

a, Workflow for UFM1 miniTurbo proximity profiling. **b**, Covalent modification of uL24 UFM1 by mT-UFM1 depends on expression of UBA5 and is enhanced by disruption of UFSP2. Immunoblot analysis of mT-UFM1 knock-in cell lines in the indicated genetic backgrounds used in the proximity labeling experiment in (**a**) and Fig. 1b. Note presence of non-specific band just above uL24-UFM1 band visible in *UBA5*^{KO}. **c**, mT-UFM1 is conjugated to uL24 on ribosomes (control for experiment in **a** and Fig. 1b). Lysates of U2OS mT-UFM1 knock-in cells treated with or without 200 nM anisomycin for 20 min to induce ribosome collisions were analyzed before (input) or after pelleting (ribosome pellet) through a sucrose cushion. **d**, Proximity labeling with mT-UFM1 shows conjugation-dependent biotinylation of proteins. Time course of UFC1 and DDRGK1 biotinylation in U2OS mT-UFM1 knock-in cells in wildtype or *UBA5*^{KO} background (as indicated) showing the conjugation-dependent specificity of biotin labeling. Cells were incubated with biotin for the indicated times prior to lysis, followed by streptavidin pulldowns (for biotinylated proteins), and elution from streptavidin beads by boiling in Laemmli buffer for immunoblot analysis. Based on the continued high selectivity for UFC1 biotinylation over the time course, mass spectrometry analysis was performed with a 4 h incubation with biotin (see Methods). **e**, Representative elutions from pull-downs as in Fig. 1b, c staining nitrocellulose with total protein stain (LI-COR Revert) or immunoblotted for uL24 to show the capture of ribosomes and enrichment of UFMylated uL24 (~80 % UFMylated). Transiently expressed eL36-SBP used to isolate ribosomes results in characteristic ribosome band patterning seen in SBP-UFM1 pulldowns, but lack bands (black arrowheads) discernable in the SBP-UFM1 pulldown that likely correspond

to UFL1 and DDRGK1 (by molecular weight). Untagged UFM1 is used as a negative control. **f**, Sucrose density sedimentation profile for experiment in (**g**). **g**, UFM1 modifies exclusively 60S *in vivo*. Lysates from wildtype K562 cells were fractionated on sucrose density gradients and analyzed by immunoblot with the indicated antibodies. Sedimentation behavior of UFMylated uL24 parallels that of the obligatory 60S markers NEMF and eIF6. **h**, Quantification of indicated bands for fractions in (**g**) showing correlations between UFMylated uL24 and NEMF (upper) and eIF6 (lower). **i**, Validation of cell lines (lanes 7-9) and UFM1 and UFSP2 distribution in fractions (lanes 1-6) used for the sucrose density sedimentation in Fig. 1d. Clonal K562 cell knockouts of UFSP2 and UFM1 show no detectable expression of UFSP2 and UFM1, respectively. Cell lysates were separated via sequential detergent fractionation into, cytosolic ("C"), and membrane ("M") fractions and analyzed by immunoblot with indicated antibodies. Non-fractionated whole cell lysate, "WC". This fractionation distinguishes the cytosolic UFC1-UFM1 adduct (an isopeptide linked conjugate) from the co-migrating uL24-UFM1 conjugate as reported previously [2,6,12]. **j**, Additional fractionation controls as in (**i**) for samples used in Fig. 1d showing partitioning of ER membrane and cytosolic markers. Membrane fractions are highly enriched for membrane markers (DDRGK1 and SEC61β) and lack cytosolic contaminants (e.g., GAPDH). **k**, Ribosome collisions increase $E3^{UFM1}$–60S association. K562 cells were treated with or without 200 nM anisomycin (ANS) for 1h to induce ribosome collisions. Lysates were sedimented through 1M sucrose to isolate ribosomes and analyzed by immunoblotting with the indicated antibodies. **l**, Quantification of mono-UFMylated uL24, UFL1, DDRGK1, and CDK5RAP3 from biological triplicates in experiment as in (**j**). Data show mean ± SD for n = 3 biological replicates. **m**, 60S ribosomes are the preferred target of UFMylation *in vitro*. Sucrose density sedimentation analysis of *in vitro* UFMylation reaction containing a 1:2 60S:80S molar ratio showing selectivity for 60S ribosome

modification. **n**, 80S ribosomes are poor substrates of UFMylation *in vitro*. Sucrose density sedimentation as in (**m**) with the same concentration of 80S ribosomes as substrate showing strongly reduced UFMylation and $E3^{UFM1}$ binding. Source data is available in Supplementary Fig. 5 (for **b**-**e** and **g**-**n**), Supplementary Table 3 (for **h**), and Supplementary Table 4 (for **l**). Data in b-e, g, k, m, and n were replicated at least twice with similar results; for detailed descriptions see "Statistics and reproducibility" section of the Methods. The mobility of molecular weight markers (in kDa) is indicated on the left hand side of the blots in panels **b-e, g, i-k, m, n.**

Extended Data Fig. 2: Coessential relationship between UFMylation and 60S recycling pathway genes.

a, The UFMylation pathway exhibits strong co-essentiality with genes involved in 60S ribosome biogenesis (green circles) and N-glycosylation genes (blue circles). All UFMylation pathway genes (yellow circles) were used as input for the FIREWORKS (https://mendillolab.shinyapps.io/fireworks/)[69] **b**, Table of DEPMAP co-dependencies for UFM1 network showing strong Pearson correlations with UFM1 pathway (yellow) and with 60S biogenesis factors EFL1, SBDS, and DNAJC21 (green). **c**, The UFL1-CTD binding site is incompatible with EFL1 and SBDS binding. Overlay of 60S-UFM1-$E3^{UFM1}$ complex in State 3 with 60S-bound SBDS and EFL1 before displacement of eIF6 (PDB 5ANB)[35]. Note that the CTD of UFL1 (orange) would sterically clash with SBDS and EFL1, suggesting that eIF6 eviction may not occur until $E3^{UFM1}$ has dissociated.

Extended Data Fig. 3: Cryo-EM data analysis and classification of native and reconstituted 60S-UFM1-$E3^{UFM1}$ complexes.

a, Data processing scheme for the native 60S-UFM1-E3^{UFM1} complex derived from a FLAG-UFM1 pulldown. 616,046 particles were picked from 11,658 micrographs using crYOLO. Following 2D classification in cryoSPARC, 83,447 particles corresponding to 60S ribosomal subunits were selected. A consensus refinement was performed followed by CTF refinement in RELION. The 60S particles were then subjected to several rounds of 3D classification using a soft mask focusing on regions where non-ribosomal extra density was observed. This revealed one stable class consisting of 14,144 particles (16,9% of all 60S particles) that was refined to an average resolution of 3.1 Å. **b**, Data processing scheme for the *in vitro* reconstituted 60S-UFM1-E3^{UFM1} complex. 1,136,353 particles were picked from 10,692 micrographs using RELION's AutoPick LoG algorithm. 2D classification revealed 846,919 ribosomal particles. 3D classification with a focused mask around the 40S revealed a number of classes, a majority of which were 60S particles with and without a bound E-site tRNA. In addition, two classes representing empty 80S ribosomes were found. Using a soft mask focusing on regions where non-ribosomal extra density was observed, one stable class consisting of 35,935 particles (4.6% of all particles) was isolated representing the stable 60S-UFM1-E3^{UFM1} complex. This class was refined to an average resolution of 2.9 Å.

Extended Data Fig. 4: Overall and local resolution and angular distribution of 60S-UFM1-E3^{UFM1} complexes.

(Local) resolution and angular distribution was assessed in RELION for the FLAG-UFM1 pulldown and the *in vitro* reconstituted sample (both resulting in State 3; see Extended Data Fig. 3) and the FLAG-UFL1 pulldown sample (yielding states 1, 2 and 3; see Extended Data Fig. 7). **a**, Gold-standard Fourier Shell Correlation (FSC) curves (obtained from RELION) for the

reconstructions of the three states obtained from the UFL1 pulldown sample (states 1-3), the *in vitro* reconstituted sample (state 3) and the UFM1-pulldown sample (also state 3). CC = correlation corrected; UM = unmasked maps; MM = masked maps; PRMM = phase randomized masked maps. **b**, Cryo-EM maps, displayed after Gaussian low-pass filtering at a standard deviation of 2 in ChimeraX and colored according to local resolution. Shown are the entire 60S-UFM1-E3^{UFM1} reconstructions (60S) as well as isolated densities for the E3^{UFM1} (E3) and the SEC61 complex (SEC61; visualized in states 1 and 2 as obtained from the FLAG-UFL1 pulldown sample). **c**, Original (unfiltered) cryo-EM maps and angular distribution plots for final 60S-UFM1-E3^{UFM1} complex reconstructions obtained from RELION. The height and color (from blue to red) of the cylinder bars is proportional to the number of particles in those views.

Extended Data Fig. 5: Models and mutational analyses of the 60S-UFM1-E3^{UFM1} complex. **a**, Final model of the UFM1-E3^{UFM1} complex derived from fitting the AlphaFold model (shown in (**b**) into the cryo-EM map of the reconstituted 60S-UFM1-E3^{UFM1} complex. This conformation represents State 3. **b**, AlphaFold model of the UFM1-E3^{UFM1} complex. In this model, the C-terminal region (480-794) of UFL1 was derived from AlphaFold 2 prediction[18] and an N-terminal fragment (1-389) was used for AlphaFold-Multimer modeling[19]. The models are colored according to a per-model confidence score (pLDDT; from 0 to 100). Blue regions display a very high confidence (pLDDT > 90), red region low confidence (pLDDT < 50). **c**, Overlay of the initial AlphaFold model (green) with the final cryo-EM model (grey). **d**, Multiple sequence alignment of the DDRGK1 UFIM and flanking regions. Intensity of color (blue/violet) represents the % sequence identity. Mutated residues in UFIM^{mt} are indicated by asterisks. Conserved residues that contact UFM1 at the C-terminal end of the DDRGK1 exit-binding helix (EBH; shown in (**e**) and

(**f**) are highlighted in red. **e,** Close-up of the DDRGK1 UFIM and EBH interactions with UFM1 derived from AlphaFold-Multimer prediction and consistent with cryo-EM density map. Side chain interactions predicted by AlphaFold-Multimer at this interface are noted. **f**, Same as (**e**), but with the amino acids that were mutated in Fig. 4d, 4h and 4i within the UFIM highlighted in purple. **g**, Crystal structure of the UFIM of UBA5 in complex with UFM1 (PDB 5IA8)[23]. Like the DDRGK1 UFIM, the UBA5 UFIM also establishes a β-augmentation with β2 of UFM1, however, neither the sequence nor the overall conformation of these UFIMs are conserved. **h,** Molecular model and schematic representation of the DDRGK1 ΔEBM mutant used in Fig. 4d, 4h and 4i. The truncated regions are depicted in gray. **i**, Molecular model and schematic representation of UFL1 C-terminal deletion mutants used in Fig. 4c. Truncated regions are depicted in gray. UFL1(1-532) = ΔCTD.

Extended Data Fig. 6: Map quality, model fitting and molecular interactions of 60S-UFM1-E3^{UFM1} complexes.

Shown are fits of the E3^{UFM1} complex model (in ribbons) into cryo-EM maps (transparent surface) of the FLAG-UFL1 native pulldown sample (States 1-3; native) and the *in vitro* reconstituted sample (state 3; in vitro). **a**, Views highlighting the interactions of the UFL1 C-terminal regions (UFL1-C) with the 60S. The maps are shown unmodified after refinement (upper row) or low-pass filtered at 5 Å (center and bottom rows) to visualize more flexible parts. Bottom row, close-up of the UFL1-C in center row; alternate angle. UFL1, yellow; 60S, grey. **b**, Views highlighting the interaction network of CDK5RAP3 and DDRGK1 with the UFL1 scaffold. Upper row; central region of the E3 complex (E3) with multiple interactions between UFL1 (yellow) and CDK3RAP5 (blue) near uL13. Lower row; UFL1/DDRGK1(magenta) interface (pHW complementation). In

state 1, these parts of the complex are not resolved. **c**, Views focusing on the DDRGK1 EBH (upper row) and close-up view on the DDRGK1 region near uL24-conjugated UFM1 (lower row; uL24, light pink; UFM1, green). Here, β-augmentation is predicted by AlphaFold formed by UFM1 and the UFIM-containing linker region between the DDRGK1 EBH and the DDRGK1 WH. The cryo-EM maps were low-pass filtered at 5 Å and show experimental evidence for predicted β-augmentation. Note that in state 1, these parts of the complex are not visualized and in states 1 and 2, the DDRGK1 EBH is not positioned. **d**, Views focusing on the structured PTC loop region (D416-V448) of the UFL1 disordered domain (N391-F479) identified near the peptidyl transferase center (PTC) of the 60S. In the best resolved density map for this region (State 3 from FLAG-UFL1 pulldown), a clear helical density is present that fits the α-helical part of the N-terminus of this region (State 3, upper right). We clearly observe densities for three basic residues (K417, R422 and R423); UFL1 Y443 engages in stacking interactions with 25S rRNA base A4548 (lower right; see also Fig, 3f).

Extended Data Fig. 7: Cryo-EM data analysis and classification of native 60S-E3^{UFM1} complexes derived from the FLAG-UFL1 pulldown.

From 50,993 micrographs, 3,017,721 particles were picked using RELION AutoPick and used for 2D classification, which yielded a total of 1,247,589 ribosomal particles. 3D classification with a mask focusing around the 40S revealed 132,004 inactive 80S ribosomes harboring eEF2 and EBP1 (ref. [55]), with the remainder of particles being 60S subunits. The 60S particles were further classified with a mask focusing around the A- and P- sites of the 60S, revealing 37,714 particles corresponding to a biogenesis intermediate featuring LSG1, NMD3, and ZNF622 (PDB 6LSR[58]). No density corresponding to the UFMylation machinery was found in this class. The remaining

particles were sorted with a mask focusing around the tunnel exit of the 60S, revealing three major subsets. One subset featured the DDRGK1 EBH and was further classified, revealing the entire E3 complex at a final resolution of 3 Å. This state was dubbed state 3. The second subset featured SEC61 bound to the 60S, and downstream classification revealed two distinct classes, one with the entire E3 bound, but with a delocalized DDRGK1 helix, and a second featuring only the C-terminal region. These states were refined to final resolutions of 3.33 and 3.27 Å, respectively, and were dubbed States 2 and 1. The last subset featured either EBP1 or no density around the tunnel exit, and further classification showed that these were empty 60S subunits.

Extended Data Fig. 8: SEC61 model fitting in States 1 and 2.

a, Three views of the SEC61 complex density from State1, low-pass filtered at 5 Å (transparent grey) with fitted model of SEC61 in closed state (PDB 6W6L)[26]. Left and center views at the C-terminal half of SEC61α including the ribosome anchor (loops 6-7 and 8-9) and the amphipathic helix of SEC61γ. This region is usually well-resolved in ribosome-SEC61 cryo-EM reconstructions and we observe helical density for transmembrane helices 5-9 of SEC61α and the N-terminal amphipathic helix of SEC61γ. Right; View at the N-terminal half of SEC61α and SEC61β. Here, the density is expectedly rather weak and only visible at very low contour levels. The N-terminal half is more flexible, especially in case the complex is not engaged with a nascent peptide substrate. **b**, **c**, Close-up views at the ribosome binding site of SEC61α, consisting of loops L6-7 and L8-9 (unfiltered density map). Here, density for these loops could be unambiguously fitted. **d-f**, same as (**a-c**), but for state 2.

Extended Data Fig. 9: UFMylation of 60S promotes SEC61 displacement.

a, **b**, Two views showing steric clashes between the N-terminal tip of the DDRGK1 EBH with SEC61 at the 60S tunnel exit site. Shown is an overlay of the DDRGK1 helix from State 3 (pink) with SEC61 from State 2 (model shown as transparent surface; SEC61α, light green; SEC61γ light blue). **c**, Mutation of the DDRGK1 UFIM reduces ribosome $E3^{UFM1}$-60S association. Representative immunoblot analysis of ribosome pellets or inputs from *DDRGK1*^{KO} HEK293 cells transiently replaced with indicated DDRGK1 variants. UFMylation was stimulated with anisomycin to enhance the detection of the low abundance E3-ribosome association. **d**, Quantification of UFL1 and CDK5RAP3 band intensities of ribosome pellets as in (**c**) from biological triplicates. Data show mean ± SD relative to *DDRGK1*^{KO} HEK293 rescued with WT DDRGK1. P values in plots for the indicated comparisons were derived from one-way ANOVA and Dunnett's multiple comparison tests for n = 3 biological replicates. **e**, **f**, 60S-UFM1-$E3^{UFM1}$ complexes sterically clash with the outer leaflet of the ER membrane. Cryo-EM maps for State 2 (**e**) and State 3 (**f**) 60S-UFM1-$E3^{UFM1}$ complexes were fitted into cryo-ET maps of mammalian ER-membrane-bound 80S ribosomes (EMD-0084)[24] to obtain an outline of the lipid bilayer (gray dashed lines). The observed position of UFM1 and the bound $E3^{UFM1}$ would partially clash with the ER membrane in State 2 requiring a slight tilt of the ribosome at the SEC61-ribosome junction to accommodate stable E3 association. In State 3, the DDRGK1 EBH would reach deep into the lipid bilayer and could only be accommodated with a substantial tilt or full dissociation of the ribosome from the SEC61 complex. **g**, Quantification of SEC61α band intensities in ribosome pellets, as in Fig. 4e. Data show mean ± SD relative to untreated and p values from indicated comparisons derived from a two-way ANOVA followed by uncorrected Fisher's LSD for *n* = 2 biological replicates. **h**, Quantification of SEC61α band intensities in ribosome pellets, as in 4f. Data show mean ± SD relative to untreated and p values from indicated comparisons derived

from a two-way ANOVA followed by uncorrected Fisher's LSD for $n = 3$ biological replicates. **i**, UFMylation is required for timely dissociation of 60S from translocon following translation termination. Immunoblot analysis of ribosome pellets or inputs from WT or *UFM1*^{KO} HEK293 cells treated with 3.75μM harringtonine for the indicated times. Quantification of SEC61α or SEC61β band intensities in ribosome pellets, as in 4e, f. Data show mean ± SD relative to untreated and p values from indicated comparisons derived from a two-way ANOVA followed by uncorrected Fisher's LSD for $n = 3$ biological replicates. Source data is available in Supplementary Fig. 6 (for **c**-**d** and **g**-**i**) and Supplementary Tables 5, 6, 7, and 8 (for **d**, **g**, **h** and **i**, respectively). All experiments were replicated at least twice; for p values and detailed descriptions of data replications see "Statistics and reproducibility" section of the Methods. The mobility of molecular weight markers (in kDa) is indicated on the left hand side of the blots in panels **c** and **i.**

Extended Data Table 1: Cryo-EM data collection, refinement and model validation. Table showing data collection, processing and refinement statistics for the five cryo-EM reconstructions and resulting molecular models presented in this work

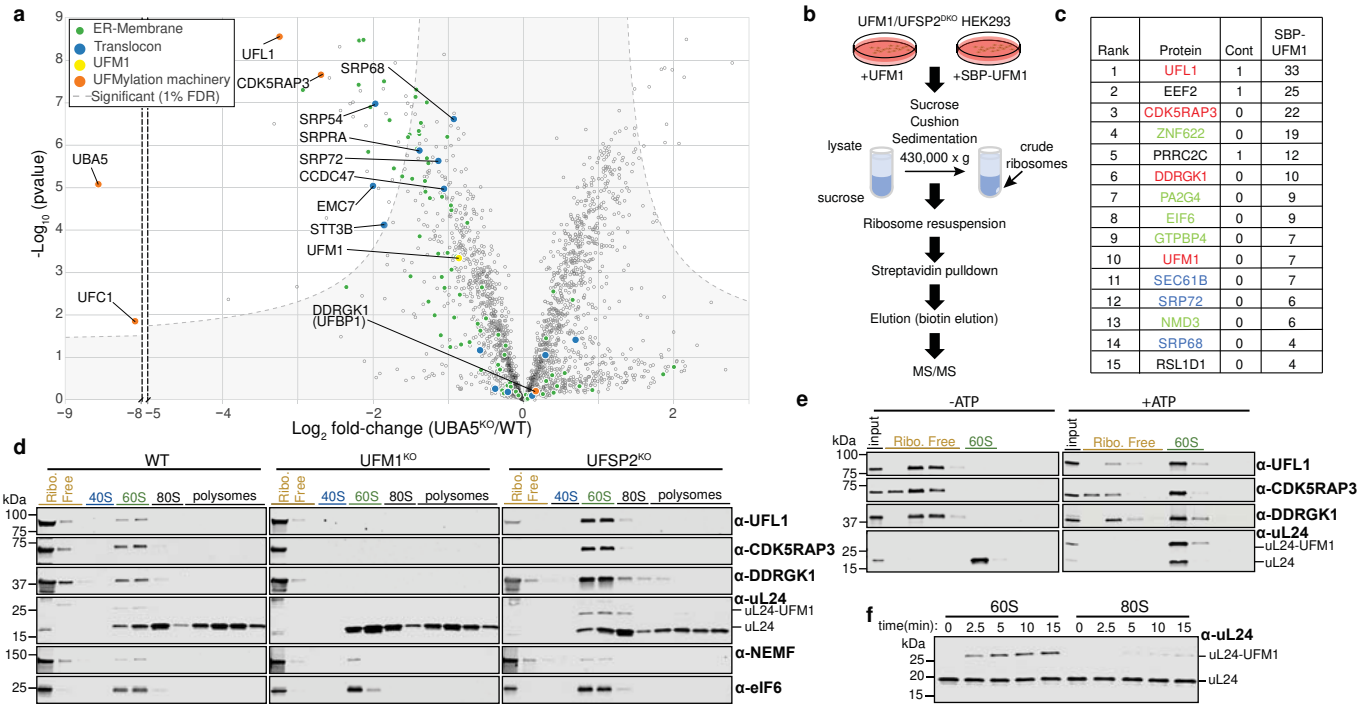
a
ER-Membrane
Translocon
UFM1
UFMylation machinery
Significant (1% FDR)
UFL1
CDK5RAP3
SRP68
SRP54
SRPRA
SRP72
CCDC47
EMC7
STT3B
UFM1
UBA5
UFC1
DDRGK1
(UFBP1)
-Log10 (pvalue)
Log2 fold-change (UBA5KO/WT)
b
UFM1/UFSP2DKO HEK293
+UFM1
+SBP-UFM1
Sucrose
Cushion
Sedimentation
lysate
430,000 x g
crude
ribosomes
sucrose
Ribosome resuspension
Streptavidin pulldown
Elution (biotin elution)
MS/MS
c
Rank | Protein | Cont | SBP-UFM1
1 | UFL1 | 1 | 33
2 | EEF2 | 1 | 25
3 | CDK5RAP3 | 0 | 22
4 | ZNF622 | 0 | 19
5 | PRRC2C | 1 | 12
6 | DDRGK1 | 0 | 10
7 | PA2G4 | 0 | 9
8 | EIF6 | 0 | 9
9 | GTPBP4 | 0 | 7
10 | UFM1 | 0 | 7
11 | SEC61B | 0 | 7
12 | SRP72 | 0 | 6
13 | NMD3 | 0 | 6
14 | SRP68 | 0 | 4
15 | RSL1D1 | 0 | 4
d
WT
UFM1KO
UFSP2KO
Ribo. Free
40S
60S
80S
polysomes
kDa
α-UFL1
α-CDK5RAP3
α-DDRGK1
α-uL24
uL24-UFM1
uL24
α-NEMF
α-eIF6
e
-ATP
+ATP
Input
Ribo. Free
60S
α-UFL1
α-CDK5RAP3
α-DDRGK1
α-uL24
uL24-UFM1
uL24
f
60S
80S
time(min): 0 2.5 5 10 15 0 2.5 5 10 15
α-uL24
uL24-UFM1
uL24

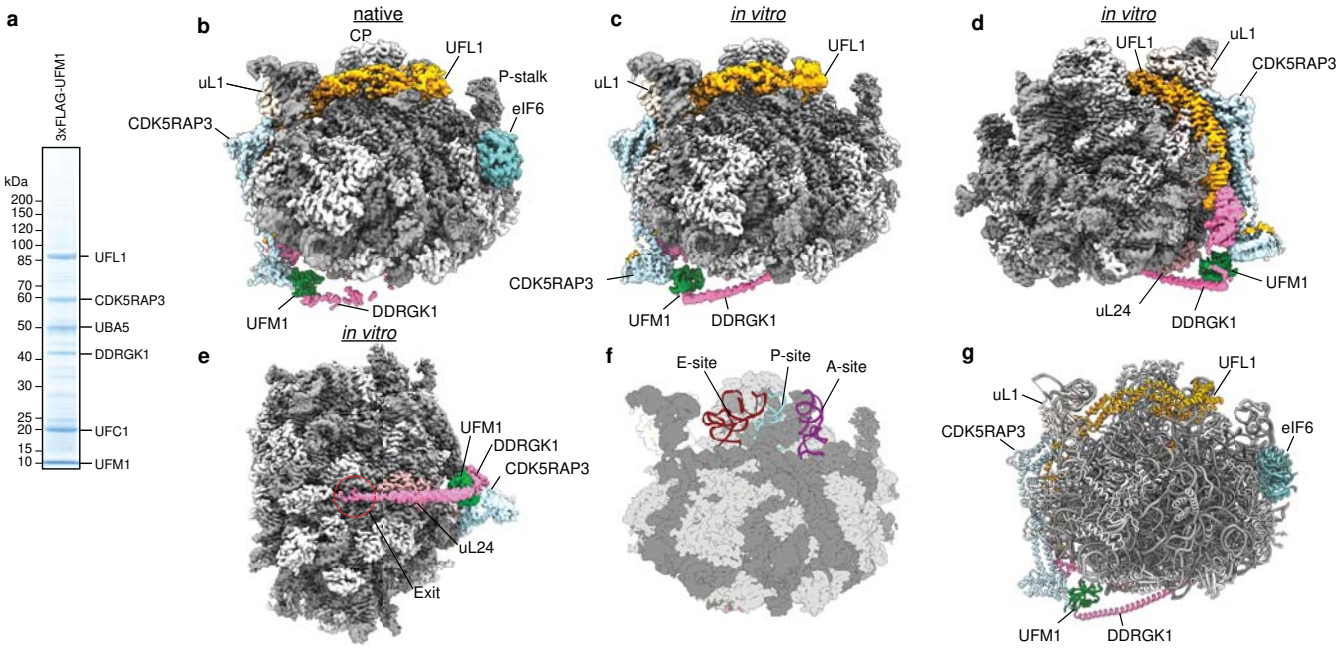
a
3xFLAG-UFM1
kDa
200
150
120
100
85
70
60
50
40
30
25
20
15
10
UFL1
CDK5RAP3
UBA5
DDRGK1
UFC1
UFM1
b
native
CP
UFL1
uL1
P-stalk
eIF6
CDK5RAP3
UFM1
DDRGK1
c
in vitro
UFL1
uL1
CDK5RAP3
UFM1
DDRGK1
d
in vitro
UFL1
uL1
CDK5RAP3
UFM1
uL24
DDRGK1
e
in vitro
UFM1
DDRGK1
CDK5RAP3
uL24
Exit
f
E-site
P-site
A-site
g
UFL1
uL1
CDK5RAP3
eIF6
UFM1
DDRGK1

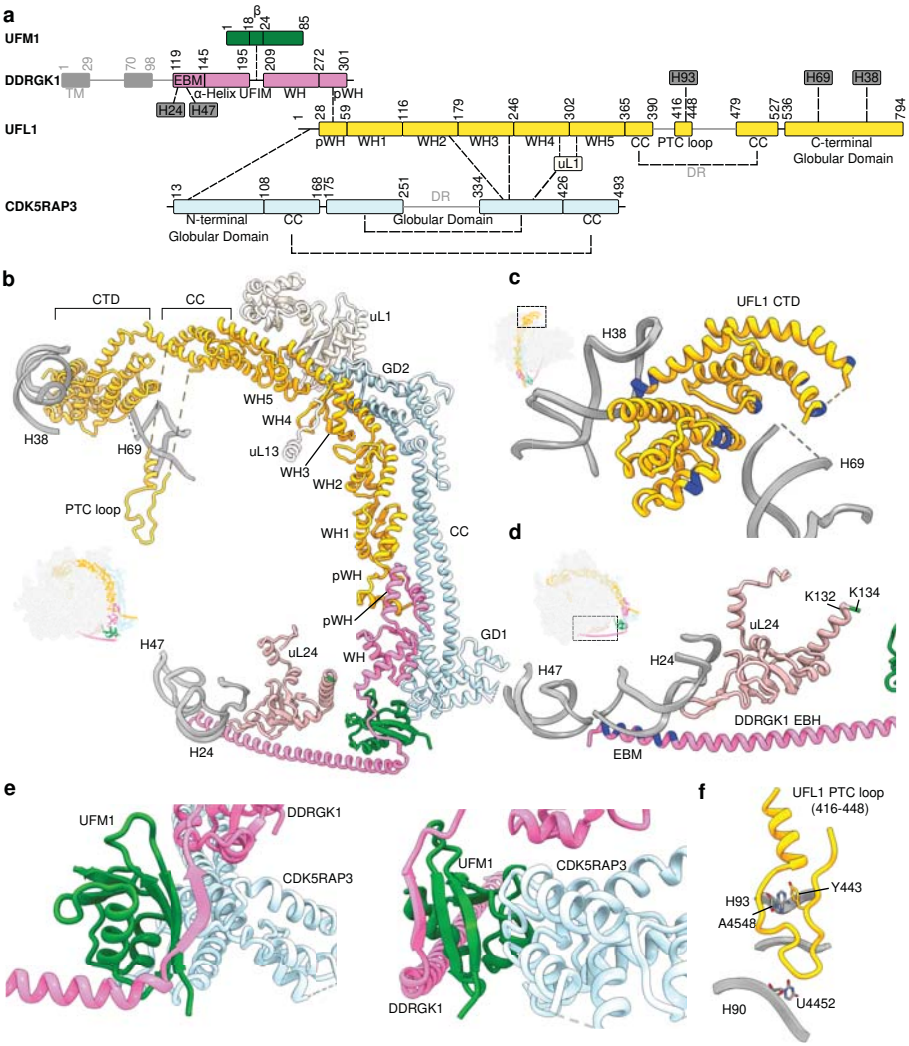
a
UFM1
DDRGK1
UFL1
CDK5RAP3
TM
EBM
α-Helix
UFIM
WH
pWH
H24
H47
H93
H69
H38
pWH
WH1
WH2
WH3
WH4
WH5
CC
PTC loop
uL1
DR
C-terminal Globular Domain
N-terminal Globular Domain
Globular Domain
b
CTD
CC
uL1
GD2
WH5
WH4
uL13
WH3
WH2
H38
H69
PTC loop
WH1
CC
pWH
pWH
GD1
H47
uL24
WH
H24
c
UFL1 CTD
H38
H69
d
K132
K134
uL24
H24
H47
DDRGK1 EBH
EBM
e
UFM1
DDRGK1
CDK5RAP3
UFM1
CDK5RAP3
DDRGK1
f
UFL1 PTC loop (416-448)
H93
Y443
A4548
H90
U4452

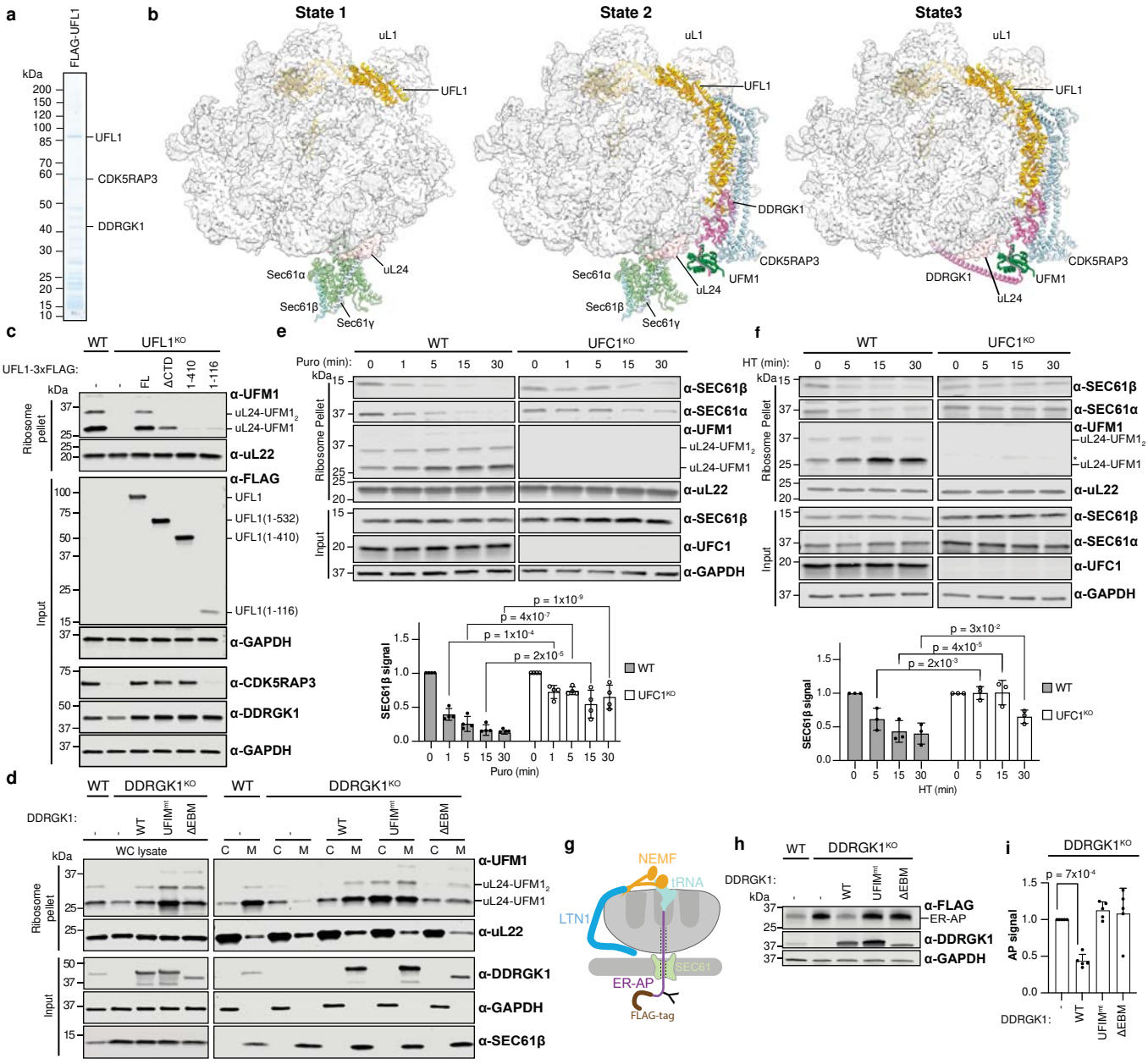
a
FLAG-UFL1
kDa
200
150
120
100
85
70
60
50
40
30
25
20
15
10
UFL1
CDK5RAP3
DDRGK1
b
State 1
State 2
State3
uL1
UFL1
DDRGK1
CDK5RAP3
UFM1
uL24
Sec61α
Sec61β
Sec61γ
c
WT
UFL1KO
UFL1-3xFLAG:
FL
ΔCTD
1-410
1-116
Ribosome pellet
Input
α-UFM1
uL24-UFM1₂
uL24-UFM1
α-uL22
α-FLAG
UFL1
UFL1(1-532)
UFL1(1-410)
UFL1(1-116)
α-GAPDH
α-CDK5RAP3
α-DDRGK1
d
WT
DDRGK1KO
DDRGK1:
WT
UFIMmt
ΔEBM
WC lysate
C
M
α-SEC61β
e
Puro (min):
UFC1KO
α-SEC61α
α-UFC1
SEC61β signal
p = 1x10-9
p = 4x10-7
p = 1x10-4
p = 2x10-5
Puro (min)
f
HT (min):
p = 3x10-2
p = 4x10-5
p = 2x10-3
HT (min)
g
NEMF
tRNA
LTN1
SEC61
ER-AP
FLAG-tag
h
α-FLAG
ER-AP
α-DDRGK1
α-GAPDH
i
AP signal
p = 7x10-4

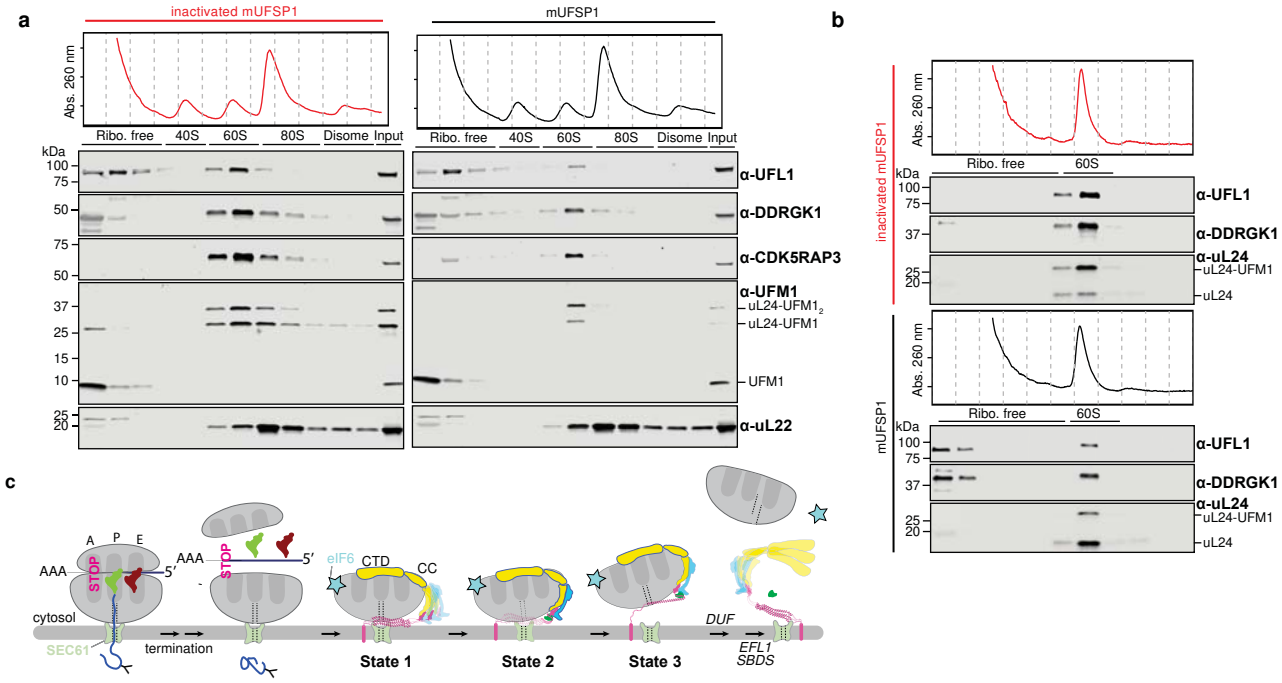
a
inactivated mUFSP1
mUFSP1
Abs. 260 nm
Ribo. free
40S
60S
80S
Disome
Input
kDa
α-UFL1
α-DDRGK1
α-CDK5RAP3
α-UFM1
uL24-UFM1$_2$
uL24-UFM1
UFM1
α-uL22
b
inactivated mUFSP1
mUFSP1
α-UFL1
α-DDRGK1
α-uL24
uL24-UFM1
uL24
c
A
P
E
AAA
STOP
5′
cytosol
SEC61
termination
eIF6
CTD
CC
State 1
State 2
State 3
DUF
EFL1
SBDS